DYNAMIC MODELING ISSUES

FOR POWER SYSTEM APPLICATIONS

A Thesis

by

XUEFENG SONG

Submitted to the Office of Graduate Studies of
Texas A&M University
in partial fulfillment of the requirements for the degree of

MASTER OF SCIENCE

December 2003

Major Subject: Electrical Engineering

DYNAMIC MODELING ISSUES

FOR POWER SYSTEM APPLICATIONS

A Thesis

by

XUEFENG SONG

Submitted to Texas A&M University
in partial fulfillment of the requirements
for the degree of

MASTER OF SCIENCE

Approved as to style and content by:

Garng M. Huang (Chair of Committee)	
Ali Abur (Member)	Henry F. Taylor (Member)
Du Li (Member)	Chanan Singh (Head of Department)

December 2003

Major Subject: Electrical Engineering

ABSTRACT

Dynamic Modeling Issues

for Power System Applications. (December 2003)

Xuefeng Song, B.S., Shandong University;

M.E., Dalian Maritime University

Chair of Advisory Committee: Dr. Garng M. Huang

Power system dynamics are commonly modeled by parameter dependent nonlinear differential-algebraic equations (DAE) $\dot{x} = f(x, y, p)$ and $0 = g(x, y, p)$. Due to the algebraic constraints, we cannot directly perform integration based on the DAE. Traditionally, we use implicit function theorem to solve for fast variables *y* to get a reduced model in terms of slow dynamics locally around *x* or we compute *y* numerically at each *x*. However, it is well known that solving nonlinear algebraic equations analytically is quite difficult and numerical solution methods also face many uncertainties since nonlinear algebraic equations may have many solutions, especially around bifurcation points. In this thesis, we apply the singular perturbation method to model power system dynamics in a singularly perturbed ODE (ordinary-differential equation) form, which makes it easier to observe time responses and trace bifurcations without reduction process. The requirements of introducing the fast dynamics are investigated and the complexities in the procedures are explored. Finally, we propose PTE (Perturb and Taylor's expansion) technique to carry out our goal to convert a DAE to an explicit state space form of ODE. A simplified unreduced Jacobian matrix is also

introduced. A dynamic voltage stability case shows that the proposed method works well without complicating the applications.

To my family

ACKNOWLEDGMENTS

I would like to thank my advisor, Dr. Garng M. Huang, for his continuous guidance, support and encouragement throughout my thesis work. I am thankful to my committee members Dr. Ali Abur, Dr. Henry F. Taylor, and Dr. Du Li for their help and time.

TABLE OF CONTENTS

LIST OF FIGURES

FIGURE Page

FIGURE Page

LIST OF TABLES

CHAPTER I

INTRODUCTION

In the last two decades, power systems have been operated under much more stressed conditions than in the past. This is largely due to the environmental pressures on transmission expansion, increased electricity consumption in heavy load areas, new system loading patterns for the deregulated electricity market, etc. Under these stressed conditions, a power system can exhibit a new type of dynamic unstable behaviors such as slow voltage drops, or even voltage collapse [1], [2], [3]. Therefore, the need for power system dynamic analysis has grown significantly in recent years.

The objective of this thesis is studying the dynamic modeling issues of power systems. We will propose improved and approximated modeling approaches, as well as power system examples to demonstrate the approaches and their applications.

1.1 Overview of Dynamic Modeling Issues of Power Systems

Power system dynamics are commonly expressed in a differential-algebraic equation (DAE) form [1], [4]

$$\begin{cases} \dot{x} = f(x, y, p), & f : \Re^{n+m+q} \to \Re^{n} \quad (1.1) \\ 0 = g(x, y, p), & g : \Re^{n+m+q} \to \Re^{m} \quad (1.2) \end{cases}$$

$$x \in X \subset \Re^{n},\ y \in Y \subset \Re^{m},\ p \in P \subset \Re^{k}$$

This thesis follows the style of the *IEEE Transactions on Automatic Control.*

where the parameter p defines specific system configurations and operation conditions, such as loads, generation, voltage setting points, etc. The dynamic state x (slow modes) describes the generation dynamics of power systems, such as exciter control systems. The instantaneous variables y (fast modes) satisfies algebraic constraints (1.2), such as power flow equations, which is implicitly assumed to have an instantaneously converging transient.

We analyze power system dynamics through observing time responses and eigenvalue solutions [3]. However, it is difficult to analyze and simulate the nonlinear DAE due to the instantaneous dynamic nature of algebraic constraints, which is only true in the approximation sense. Traditionally, we use implicit function theorem to solve for fast variables y to get a reduced model in terms of slow dynamics locally around x. Or we compute y numerically at each x. The reduced Jacobian matrix of DAE is often used in the analysis of power system dynamics [3], [5]. The linearized dynamic expression of DAE is as below [1], [6]:

$$\begin{bmatrix} \Delta\dot{x} \\ 0 \end{bmatrix} = J_u \begin{bmatrix} \Delta x \\ \Delta y \end{bmatrix} \tag{1.3}$$

$$J_u = \begin{bmatrix} f_x & f_y \\ g_x & g_y \end{bmatrix} \tag{1.4}$$

DAE (1.3) can be reduced to an ODE (ordinary-differential equation) when g_y is nonsingular, i.e., the algebraic variable Δy can be eliminated from (1.3) [1]

$$\Delta\dot{x} = [f_x - f_y g_y^{-1} g_x]\Delta x = J_r \Delta x \tag{1.5}$$

$$J_r = [f_x - f_y g_y^{-1} g_x] \tag{1.6}$$

where J_r is called the reduced Jacobian matrix (RJM) as opposed to the unreduced Jacobian matrix (UJM) J_u. The stability of an equilibrium point of the DAE system for a given p depends on the eigenvalues of the reduced Jacobian matrix J_r [1]. Through tracing the eigenvalues of matrix J_r, we can study the local dynamic stability of the systems [1], [7]. There are two steps involved to identify the dynamic stability of power systems as the parameter p slowly changes. First, solve and trace the equilibrium point along the path, which is defined by a scheduled system operating strategy. Then, form RJM and analyze the eigenvalues at each equilibrium point [1], [8], [9].

The reduction computation may not be trivial. It is well known that solving nonlinear algebraic equations analytically is quite difficult. Numerical methods can be used to solve DAE systems. The procedure involves alternately solving the algebraic power flow equations representing the network and the differential equations representing the machines [6], [10]. We may use Gauss-Seidel (or Newton-Raphson) method to solve nonlinear algebraic equations (power flow equations) and Euler's method (or Runge-Kutta method) to get the solutions of differential equations [10]. The integration and algebraic solving are alternately applied and the procedure is messy. For large power systems, if the initial condition is far from a solution point of the power flow or the power flow problem is an ill-conditioned one, convergence of the power flow solutions can be significantly slow or does not exist at all [11]. In addition, algebraic constraints are approximations of fast dynamics, which assumes that the fast variable converges to its equilibrium state instantaneously. Even if this is almost true, the

approximation may make its dynamic response too fast to be observed and the interaction between fast modes and slow modes may become unclear.

Compared to RJM, the unreduced Jacobian matrix (UJM) J_u in (1.4) is simpler and attractive to use in power system applications. Unfortunately, using this J_u may not be able to obtain the exact system dynamic behaviors due to the unknown fast dynamics $\dot{y}$. The singular perturbation provides a way to deal with this issue [8], [12]. Paper [8] uses sign adjustment to model power system dynamics where a UJM is used in bifurcation analysis. However it is difficult for cases with high dimensional power flow constraints. In addition, decision on sign change is a big computation burden itself. Paper [12] derives an approximated expression of fast dynamics but does not analyze the dynamics based on the approximation in details. When it is used in the dynamic voltage stability studies, we find that the singularity-induced bifurcation (SIB) of the original DAE system is not preserved. The eigenvalue loci near the singular point are quite different from those of the original DAE system. All these make the approximation questionable.

1.2 Objectives and Organization of This Thesis

In this thesis, we introduce our new approach to model power system dynamics in a singularly perturbed ODE, which can be directly integrated to obtain time responses to avoid solving the nonlinear algebraic equations. The bifurcation properties of the original DAE system are preserved by the ODE.

The idea of our new modeling approach is based on the following considerations:

Singular perturbation is particularly suitable for modeling interacting dynamics with large separation phenomena in their speed [4], [13]. Power system dynamics has a two-time scale that indicates we can apply singular perturbation to model a DAE system in a singularly perturbed ODE form. The standard form of a singular perturbation problem is [13]

$$\begin{cases} \dot{x} = f(x, y, p, \varepsilon) & x \in \Re^n \quad (1.7) \\ \varepsilon \dot{y} = g^{FD}(x, y, p, \varepsilon) & y \in \Re^m \quad (1.8) \end{cases}$$

where the small positive scalar ε called *perturbation parameter* represents the ratio of time scales associated with slow dynamics $\dot{x}$ and fast dynamics $\dot{y}$ [4], [13]. Based on the singular perturbation, one way to handle the algebraic constraints is to slow down the fast modes by introducing fast dynamics (1.8) instead of the algebraic equations (1.2). Thus the DAE of power system dynamics is converted to a singularly perturbed ODE. Numerical integration techniques can be directly applied to obtain approximate solutions of the nonlinear ordinary-differential equations. In the procedure, we do not solve the nonlinear algebraic equations to obtain the initial power flow solutions at each of the iterative step; and the alternative procedures to solve the DAE [10] are avoided. Given an initial point of x and y, we use either Euler's method or Runge-Kutta method to integrate the ODE to get the time domain solutions [12]. For a large-scale power system, our new approach will take less calculation time since solving the power flow equation is avoided. The dynamic behaviors of power system described by DAE can be quickly evaluated by integrating the ODE without solving the power flow solutions.

Therefore, the objectives of this thesis are:

- Remodel the DAE by a singularly perturbed ODE to avoid solving the nonlinear algebraic equations so that we can directly integrate the ODE without reduction process.
- Investigate the requirements and explore the complexities to introduce the fast dynamics.
- Propose PTE (Perturb and Taylor's Expansion) technique to build the fast dynamics. Thus, by PTE, a DAE is converted to a singularly perturbed ODE.

The organization of the thesis is as below:

- In chapter II, we present fundamental insights of our modeling approach. A detailed dynamic analysis of a DAE system is demonstrated and compared with the singularly perturbed ODE form. We then investigate the requirements and explore the complexities of applying our new modeling approach. Some associated mathematical background materials on bifurcation analysis are provided.
- In chapter III, we present the technique of PTE (Perturb and Taylor's Expansion) to derive a generic expression of fast dynamics. A simplified unreduced Jacobian matrix is also proposed which can be used in the eigenvalue analysis. A power system example is given to demonstrate our proposals.
- Finally, all conclusions will be presented in chapter IV.

CHAPTER II

ISSUES OF DIFFERENTIAL-ALGEBRAIC EQUATION (DAE) MODELING

In this chapter, we present fundamental insights of our modeling approach. A detailed dynamic analysis of a DAE system is demonstrated and compared with our singularly perturbed ODE. We then discuss the requirements and the complexities to describe fast dynamics. A quick review of needed mathematical background is also provided. We focus on DAE systems, bifurcation analysis, and our singular perturbation approach.

2.1 Parameter Dependent DAE System

Parameter dependent DAE of the form

$$\begin{cases} \dot{x} = f(x, y, p), & f : \Re^{n+m+k} \to \Re^{n} \quad (2.1) \\ 0 = g(x, y, p), & g : \Re^{n+m+k} \to \Re^{m} \quad (2.2) \end{cases}$$
$$x \in X \subset \Re^{n},\ y \in Y \subset \Re^{m},\ p \in P \subset \Re^{k}$$

is widely used to model the dynamics of physical systems, such as dynamic voltage stability of power systems [1], [12], [14]. In the parameter-state space of *X, Y, P*, x is a vector of n state variables, y is a vector of m algebraic variables, and p is a vector of k parameter variables, which are changing slowly. The m algebraic equations (2.2) define an $n+k$ dimension manifold, called *constraint manifold*, in the $n+m+k$ dimensional parameter-state space of *X, Y, P*. System equilibrium points (x_e, y_e) satisfying

$$\begin{cases} 0 = f(x_e, y_e, p) & (2.3) \\ 0 = g(x_e, y_e, p) & (2.4) \end{cases}$$

define a *k*-dimensional *equilibrium manifold* in the state space of *X*, *Y*. Due to the algebraic constraints, we cannot directly perform integration on the DAE form. Traditionally, we use the implicit function theorem to eliminate fast variable *y* to get a reduced model in terms of slow dynamics *x*. Consider a point *x, y, p* for which the algebraic Jacobian g_y (i.e. $\partial g / \partial y$) is nonsingular, according to the implicit function theorem, there exists a locally unique, smooth function *F* [4], [15]

$$\dot{x} = F(x, p) \tag{2.5}$$

where the algebraic variables *y* have been eliminated.

However, it is not trivial to get the reduced model (2.5) due to the nonlinear algebraic equations. There are computational burdens involved in the reduction process: We may solve y in terms of *x* and then substitute it in the slow dynamics to get the reduced model locally around *x*. Or we may compute *x* and *y* alternatively using numerical integration and solving algebraic equations, which is time consuming. In the analysis of nonlinear system dynamics, linearization is often used to get a local picture of dynamic behaviors around an equilibrium point of a nonlinear system. For the DAE, at equilibrium point (x_e, y_e), defining

$$\Delta x = x - x_e, \qquad \Delta y = y - y_e \tag{2.6}$$

The linearized DAE is expressed as below:

$$\begin{bmatrix} \Delta \dot{x} \\ 0 \end{bmatrix} = J_u \begin{bmatrix} \Delta x \\ \Delta y \end{bmatrix} \tag{2.7}$$

where J_u is denoted as the unreduced Jacobian of the DAE system

$$J_u = \begin{bmatrix} f_x & f_y \\ g_x & g_y \end{bmatrix} \tag{2.8}$$

When g_y is nonsingular, we eliminate Δy from (2.7) to get the reduced model as following:

$$\Delta \dot{x} = J_r \Delta x \tag{2.9}$$

where

$$J_r = [\, f_x - f_y g_y^{-1} g_x \,]\Big|_{(x_e, y_e)} \tag{2.10}$$

J_r is the reduced Jacobian matrix (RJM) of the DAE system. As seen in (2.9), the DAE is reduced to an *n*-dimensional ODE. As *p* changes slowly, we solve for the system equilibrium points and build the reduced Jacobian matrix for each of the equilibrium points. The dynamic behaviors of an equilibrium point can be analyzed through the eigenvalues of the reduced Jacobian J_r evaluated at the equilibrium point.

In contrast to linear systems, in a nonlinear system we should always be aware of the following facts [4], [15]:

- A nonlinear system may have one or more than one or no equilibria.
- The region of attraction of a stable equilibrium point may be limited.

2.2 Bifurcation Analysis

Bifurcation analysis is widely used in nonlinear system dynamic studies [14]. As *p* varies slowly in the parameter space, we trace system equilibrium points and the

corresponding eigenvalues through RJM to observe bifurcations of parameter dependent DAE systems [1], [16]. In this section we will briefly introduce the ideas behind bifurcation analysis.

Consider a nonlinear system represented by [4], [15]

$$\dot{x} = f(x, p) \tag{2.11}$$

where x is an n×1 vector and p is a k×1 parameter vector. For every value of p the equilibrium points of the system are given by the solution of:

$$f(x, p) = 0 \tag{2.12}$$

Consider an equilibrium point $x^{(1)}$ corresponding to the parameter p_0, and assume that the Jacobian of f is nonsingular at this point

$$\det f_x(x^{(1)}, p_0) \neq 0 \tag{2.13}$$

By the implicit function theorem, there exists a unique function

$$x^* = g^{(1)}(p) \tag{2.14}$$

such that

$$x^{(1)} = g^{(1)}(p_0) \tag{2.15}$$

gives a branch of equilibrium points of system (2.11) as a function of p.

Similarly, for the same value p_0 it may exist many equilibrium points, say $x^{(2)}$, i.e. another solution of (2.12). This solution also corresponds to a nonsingular Jacobian $f_x(x^{(2)}, p_0)$. By the implicit function theorem, we have a second function

$$x^* = g^{(2)}(p) \tag{2.16}$$

such that

$$x^{(2)} = g^{(2)}(p_0) \tag{2.17}$$

gives another branch of equilibrium points of system (2.11) as a function of p.

As p varies, the bifurcation occurs when different branches of equilibrium points intersecting each other, and thus either bifurcating or disappearing [4], [14], [15]. Note, in such bifurcation points the Jacobian f_x becomes singular, and consequently the implicit function theorem is no longer valid [4].

Here an example illustrates the bifurcation concept:

$$\dot{x} = (x-1)^2 + p \tag{2.18}$$

The equilibrium points satisfy

$$(x-1)^2 + p = 0$$

where p is a scalar parameter (k=1). This system has two equilibrium points for p<0, a single equilibrium for p=0 and no equilibrium points for p>0. In Fig. 1 we see that two branches of equilibrium points $x^{(1)}(p)$ and $x^{(2)}(p)$ on the plane (p, x) intersect at the bifurcation point B. At this point the following conditions are satisfied:

$$p = 0, \quad x^* = 1, \quad \frac{\partial f}{\partial x} = 2(x^* - 1) = 0 \tag{2.19}$$

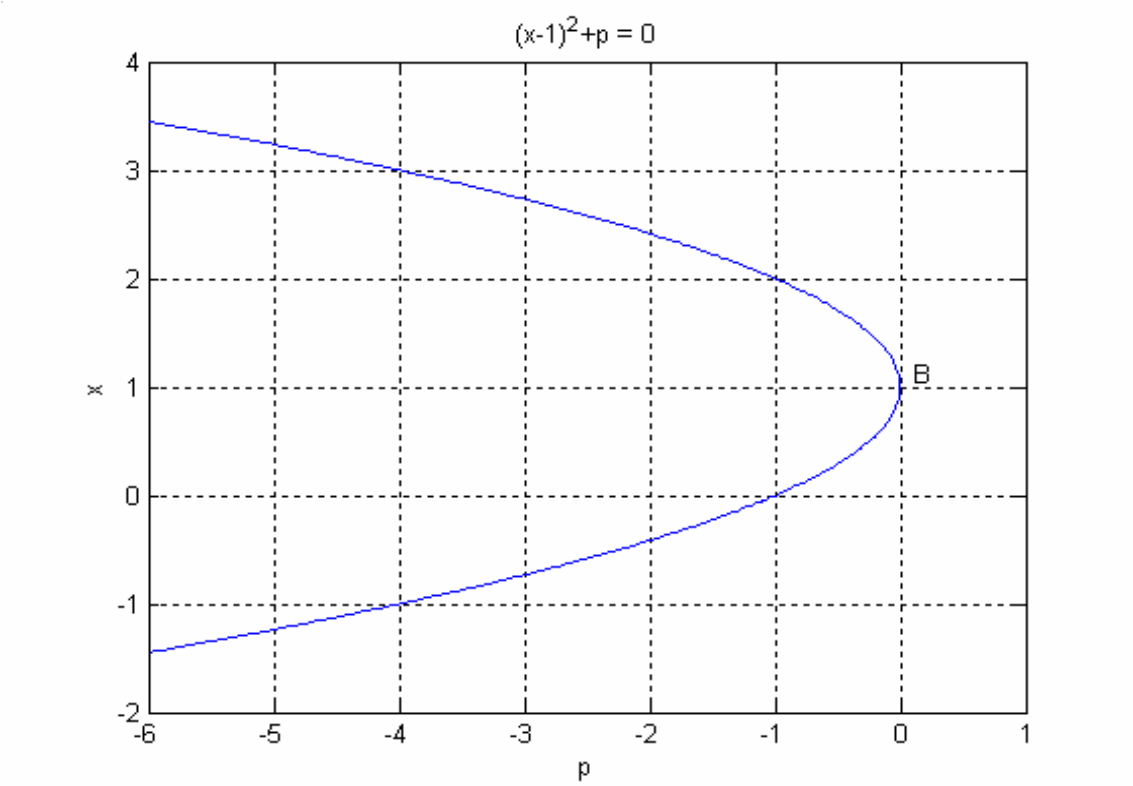

Fig. 1. An illustration of a bifurcation point.

In general, bifurcations may occur at any point along the parameterized path [17]. It is an important characteristic that the qualitative structure of the system (2.11) will change drastically by a small perturbation of p at a bifurcation point [4], [17]. Accordingly, these bifurcation points are critical points for dynamic stability analysis of nonlinear systems, which deal with local properties such as the dynamic stability of equilibrium points under small variations of parameter p [18]. Three types of bifurcations are encountered in bifurcation analysis of power system dynamics [4], [19]: Saddle-Node Bifurcation (SNB), Hopf Bifurcation (HB), and Singularity-Induced Bifurcation (SIB).

2.2.1 Saddle-Node Bifurcation (SNB)

An SNB is a point where a pair of equilibria, meets and disappears with a zero eigenvalue [15]. One of the equilibria (node) is stable while the other (saddle) is unstable. The particular point is referred to as a *saddle-node bifurcation* [15]. Like the case described in Fig. 1, for $p<0$, there are two distinct equilibrium points, one stable and the other unstable. These two equilibria coalesce as $p=0$ and disappear as $p>0$. In this sense, point B is a saddle-node bifurcation of the first order system. At point B the Jacobian (2.19) is singular. Near the saddle-node there exists a direction, along which trajectories behave as shown in Fig. 2, approaching the equilibrium from the one side (stable manifold of the SNB), and diverging on the other (unstable manifold of the SNB) [4]. Moreover, B is an unstable equilibrium point lying on the stability boundaries at the critical parameter value $p=0$.

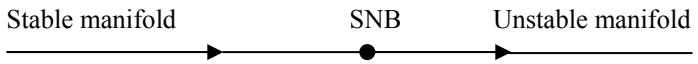

Fig. 2. Saddle-node.

For a general n-dimensional system we have the following conclusion [4], [17], [15]:

At a Saddle-Node Bifurcation, two equilibrium points, one has a real positive and the other a real negative eigenvalue, coalesce and disappear both the eigenvalues becoming zero at the bifurcation.

In a saddle-node bifurcation, the region of attraction of the stable equilibrium point shrinks due to an approaching the unstable equilibrium point and the stability is eventually lost when the two equilibria coalesce and disappear [15]. This implies that an SNB has a Jacobian with a simple zero eigenvalue. The saddle-node bifurcation has been linked to voltage collapse in [1], [8], [9], [17], and [20]. An important feature of the saddle-node bifurcation is the disappearance, locally, of any stable bounded solution of the dynamic system [21].

2.2.2 Hopf Bifurcation (HB)

As we know, an SNB is characterized by a zero eigenvalue at the origin of the complex plane. There is another type of stable equilibrium points that can become unstable following a parameter variation that force a pair of complex eigenvalues to cross the imaginary axis in the complex plane [15]. This type of oscillatory instability is associated in nonlinear systems with the Hopf Bifurcation (HB). Fig. 3 shows the loci of the eigenvalues near the Hopf bifurcation point.

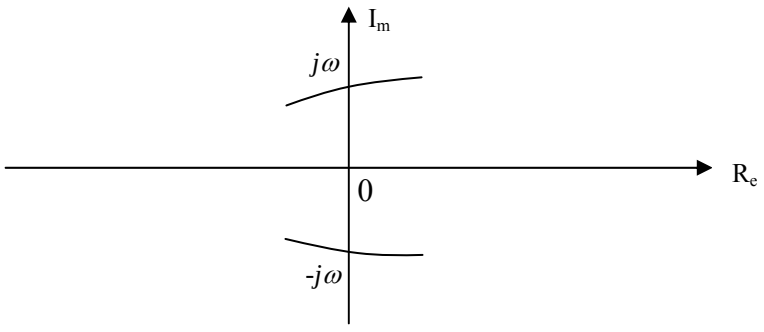

Fig. 3. Purely imaginary eigenvalues ($\lambda=\pm j\omega$) occur at Hopf bifurcation.

In Fig. 3, a Hopf bifurcation occurs at a point where the system has a simple pair of purely imaginary eigenvalues ($\lambda=\pm j\omega$) and no other eigenvalue with zero real part. Hopf bifurcations signal the birth or the annihilation of period orbits called limit cycle [4]. More precisely, a limit cycle is an isolated periodic solution of a nonlinear system $\dot{x} = f(x)$. Here, a periodic solution is a function $x(t)$ satisfying $\dot{x} = f(x)$ and having the property of $x(t+T) = x(t)$ for all t, where T is the period of the periodic solution. Therefore, a limit cycle is a closed curve in n-dimensional space [4].

At an HB the stability of the equilibrium point is lost through its interaction with a limit cycle [15]. It is expected that in the vicinity of this bifurcation either stable or unstable limit cycles should exist. There exist two types of Hopf Bifurcation depending on the nature of the interaction with a limit cycle [14], [15]:

Subcritical HB: an unstable limit cycle, existing prior to the bifurcation, shrinks and eventually disappears as it coalesces with a stable equilibrium point at the bifurcation. After the bifurcation, the equilibrium point becomes unstable resulting in growing oscillations.

Supercritical HB: a stable limit cycle is generated at the bifurcation, and a stable equilibrium point becomes unstable with increasing amplitude oscillations, which are eventually attracted by the stable limit cycle.

The instability mechanism of the subcritical Hopf bifurcation is shown in Fig. 4 (a) where annihilation of the operating point leads to oscillatory diverging. The

instability mechanism of the supercritical Hopf bifurcation is shown in Fig. 4 (b) where operation changes from an operating point to stable oscillations [17].

(a) (b)

Fig. 4. The instability mechanism of Hopf bifurcations [17]. (a) Subcritical Hopf bifurcation. (b) Supercritical Hopf bifurcation.

From an engineering viewpoint both cases are unacceptable since both result an unstable operating point with oscillations after this bifurcation. The necessary condition for a HB is the existence of equilibrium with purely imaginary eigenvalues. For which the real part of the critical eigenvalue pair does not change sign after going to zero are not HB points [4].

2.2.3 Singularity-Induced Bifurcation (SIB)

A special type of bifurcation called singularity-induced bifurcation (SIB) exists in DAE system [17]. The state space of DAE systems is divided into open components by surface where the Jacobian matrix of algebraic equations is singular. The surface is defined by [4]

$$\begin{cases} g(x, y, p) = 0 & (2.20a) \\ \det g_y(x, y, p) = 0 & (2.20b) \end{cases}$$

Since one more algebraic equation (2.20b) is added to the m initial ones, equations (2.20a) and (2.20b) form an $n+k$-1 dimensional surface, lying on the constraint manifold. According to the implicit function theorem, when Jacobian matrix g_y is singular, it cannot be solved for the m dependent algebraic variables y. In other words, the system cannot be defined on the singular surface. Therefore, this hypersurface is called *impasse surface*, because it cannot be crossed by the trajectories of the system [4], [15].

An SIB is defined by both singularities and equilibrium conditions, i.e., [4]

$$\begin{cases} f(x, y, p) = 0 & (2.21a) \\ g(x, y, p) = 0 & (2.21b) \\ \det g_y(x, y, p) = 0 & (2.21c) \end{cases}$$

The SIB occurs when the k dimensional equilibrium manifold, which lies on the constraint manifold of a DAE system, intersects the $n+k$-1 dimensional impasse surface. Usually, these singular points are not equilibrium points because the system cannot be defined on the impasse surface [4]. However, equilibrium points may exist arbitrarily close to both sides of such a singularity.

Consider a family of equilibrium points approaching the impasse surface under a slow parameter change. The det[g_y] becomes very small as the IS approached, and consequently the det[J_r] gets very large due to (2.10). Therefore at least one of the eigenvalues of the state matrix J_r tends to infinity. Similarly, on the other side of the IS, the equilibrium points have also an eigenvalue tending to infinity, but with an opposite

sign [1]. We have therefore a change of the stability properties of the system on the two sides of the singularity and this constitutes a bifurcation, called singularity-induced bifurcation [17], [22].

Note that in DAE systems the det[J_r] changes sign, either when it becomes singular, having a zero eigenvalue, or when it has an unbounded eigenvalue going from minus infinity to plus infinity [11], [21]. The previous one could be an SNB while an SIB for the later one.

Let us take an example to illustrate SNB and SIB:

$$\dot{x} = -yx + 2p \tag{2.22}$$

$$0 = -y^2 + y\sqrt{1-x^2} - p \tag{2.23}$$

$$x \in X \subset \Re,\ y \in Y \subset \Re,\ p \in P \subset \Re$$

where p is a positive scalar parameter. In this system, n=m=k=1. The state and parameter space X, Y, P has dimension n+m+k=3. The constraint manifold is a surface of dimension n+k=2. The impasse surface is an n+k-1=1 dimensional curve and the equilibrium manifold is another k=1 dimensional curve lying on the constraint manifold.

The 2-dimensional constraint manifold, defined by (2.23), is represented through a collection of contours shown in Fig. 5 with solid lines for different values of p. The impasse surface (IS) is defined by the constraint (2.23) and the singularity condition

$$g_y = \frac{\partial g}{\partial y} = -2y + \sqrt{1-x^2} = 0 \tag{2.24}$$

It is shown as a dash curve marked IS in Fig. 5 that divides the constraint manifold into two components. Note that each solid curve of the constraint manifold folds with respect

to the *x*-axis at its crossing point with the impasse curve. The equilibrium manifold (EM) satisfies the following conditions:

$$-yx+2p=0 \tag{2.25}$$

$$-y^2+y\sqrt{1-x^2}-p=0 \tag{2.26}$$

From above two equations, we get the curve in *X*, *Y* space

$$-y+\sqrt{1-x^2}-0.5x=0 \tag{2.27}$$

which is shown as a dash-dot line marked EM in Fig. 5.

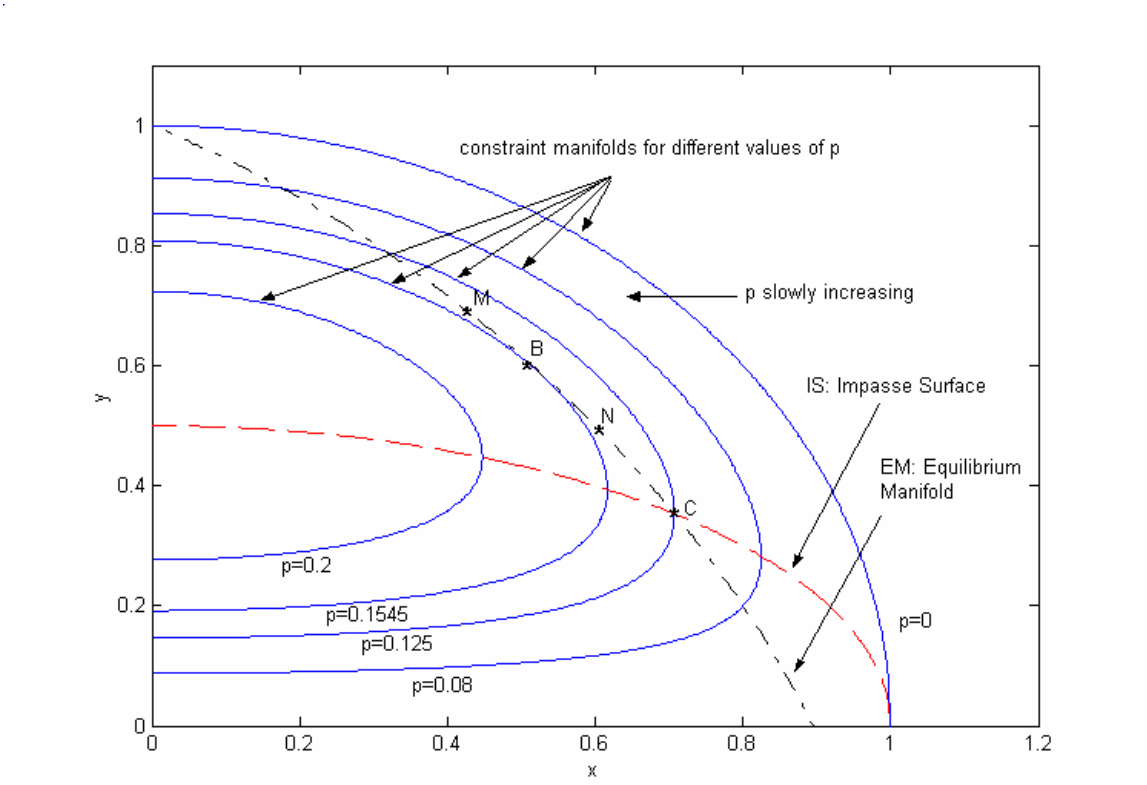

Fig. 5. C: singularity-induced bifurcation, B: saddle-node bifurcation.

As seen in Fig. 5, the equilibrium manifold EM intersects the impasse surface IS at point C, which is a singularity-induced bifurcation. We use the reduced Jacobian matrix to calculate eigenvalues in the bifurcation analysis. The linearized system around an equilibrium point is expressed as below:

$$\begin{bmatrix} \Delta \dot{x} \\ 0 \end{bmatrix} = J_u \begin{bmatrix} \Delta x \\ \Delta y \end{bmatrix} \tag{2.28}$$

$$\begin{aligned} J_u &= \begin{bmatrix} f_x & f_y \\ g_x & g_y \end{bmatrix} \\ &= \begin{bmatrix} -y & -x \\ \dfrac{-yx}{\sqrt{1-x^2}} & -2y+\sqrt{1-x^2} \end{bmatrix} \end{aligned} \tag{2.29}$$

$$\Delta \dot{x} = J_r \Delta x \tag{2.30}$$

$$\begin{aligned} J_r &= f_x - f_y g_y^{-1} g_x \\ &= -y - \frac{1}{-2y+\sqrt{1-x^2}} \left(\frac{yx^2}{\sqrt{1-x^2}} \right) \end{aligned} \tag{2.31}$$

The eigenvalue of the reduced Jacobian J_r just equals to J_r. Fig. 6 shows the eigenvalue locus as $p \rightarrow 0.125$. We can see clearly that as p close to 0.125 from one side, say $p=0.125^{-}$, the eigenvalue of J_r tends to minus infinity; as $p=0.125$, g_y is singular; after this point, say $p=0.125^{+}$, the eigenvalue of J_r tends to plus infinity. So the system

changes the property at p=0.125 which corresponds to the singularity-induced bifurcation (SIB) point C.

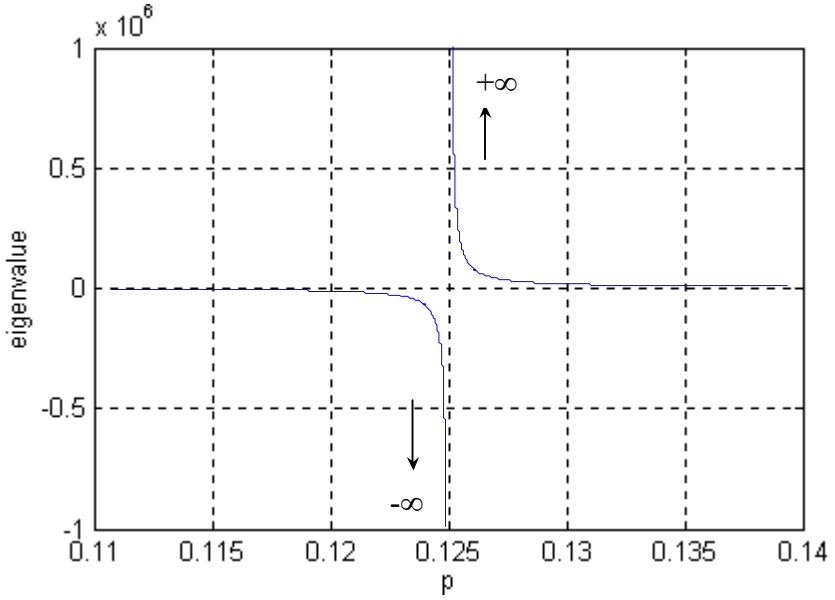

Fig. 6. Singularity-induced bifurcation as p=0.125.

For this case we can also observe the saddle-node bifurcation. Now let p varies slowly starting from 0 to seek SNB. For p=0 we have x=0, y=1. The eigenvalues of J_u are –1, –1 while the eigenvalue of J_r is –1. This is a stable equilibrium point. Increasing p slowly, we move uphill along the dash-dot equilibrium curve until reaching point B (for p slightly larger than 0.1545), after which there is no equilibrium point for increasing p. This is an SNB, at which a stable equilibrium point such as M coalesces with an unstable equilibrium point such as N, which bounds the region of attraction of the stable equilibrium point M. The descending path in the direction of N is made up of unstable equilibria becoming more and more unstable with an eigenvalue approaching

$+\infty$ at the SIB point C. There is no Hopf bifurcation since this is an n=1 dimensional system. We will observe Hopf bifurcation through a simple power system example in chapter III.

In conclusion, a bifurcation occurs when the qualitative structure of the system (i.e., the number of equilibrium points, their stability, etc.) changes for a small variation of the parameters. In the parameter dependent DAE problems, there are three generic bifurcations [2], [17]:

- Saddle-node bifurcation (SNB), where two equilibria coalesce and then disappear. At this point the Jacobian has a zero eigenvalue, i.e., it is singular.
- Hopf bifurcation (HB), where there is emergence of oscillatory instability. At this point, two complex conjugate eigenvalues of Jacobian cross the imaginary axis.
- Singularity-induced bifurcation (SIB), where g_y is singular. One eigenvalue is going to infinity at both sides of the singular point with opposite sign.

2.3 Fundamental Insights of the Modeling Approaches

Dynamics may evolve in different time scales; some are fast and others slow. It is not practical to treat both dynamics in the same way. For a DAE system, due to the algebraic constraints, we cannot directly perform integration or calculate eigenvalues. In this section, we introduce our new singular perturbation approach to solve DAE systems. Our goal is to remodel the DAE system by an ODE without reductions. Hence we can integrate directly to the ODE. The ODE should preserve bifurcation properties of the original DAE system, since the bifurcations are the critical points to determine the

stability boundaries in the parameter-state space of X, Y, P [17]. We will demonstrate it through a simple example.

As we know that, singular perturbation is suitable to model interacting dynamics with large separation in their speed. A singularly perturbed system is one for which a small parameter ε multiplies one or more state derivatives. The standard model of a singular perturbation problem is [13]

$$\begin{cases} \dot{x} = f(x, y, p, \varepsilon) & (2.32) \\ \varepsilon \dot{y} = g^{FD}(x, y, p, \varepsilon) & (2.33) \end{cases}$$

where x is an $n\times1$ vector that denotes slow dynamics, y is an $m\times1$ vector that denotes fast dynamics (FD). The parameter space p is composed of system parameters and operating parameters. A small positive scalar ε called *perturbation parameter* represents the ratio of time scales associated with slow dynamics $\dot{x}$ and fast dynamics $\dot{y}$.

When a two-time scale model (one is fast and the other slow) is available, one can derive accurate, reduced-order models suitable for each time scale. This process is called time-scale decomposition and the associated analysis is known as singular perturbation [13].

Consider the very small perturbation parameterε, the dynamics of y are faster than those of x. Thus an approximation of the slow dynamics of the original two-time scale system (2.32)-(2.33) is that of taking ε=0 in (2.33) under the following condition [4], [13]:

The fast dynamics is locally uniformly asymptotically stable.

It means that g_y^{FD} (i.e. $\partial g^{FD}/\partial y$) has all eigenvalues with strictly negative real parts, i.e., fast modes converge. It also implies that Jacobian g_y^{FD} is nonsingular and all trajectories remain in the attractive region of the stable equilibrium of the g_y^{FD} dynamics. Under this condition, when $\varepsilon = 0$, the dynamics of *y* is infinitely faster than those of *x*, the ODE (2.32)-(2.33) becomes DAE (2.34)-(2.35). The system order (*n*+*m*) is then reduced to *n,* the order of *x*.

$$\begin{cases} \dot{x} = f(x, y, p) & (2.34) \\ 0 = g^{FD}(x, y, p) & (2.35) \end{cases}$$

The slow subsystem is a differential-algebraic system that can be analyzed through the reduced Jacobian matrix J_r as described in the previous section. The slow subsystem approximates the dynamics of the original ODE system (2.32)-(2.33) well [4], [13]; and the dynamic behaviors of the system around an equilibrium point is characterized by the reduced Jacobian matrix J_r of the form (2.10).

However, power system dynamic analysis has been based on the differential-algebraic equations of the form (2.34)-(2.35). The algebraic constraints result from approximating the fast dynamics as instantaneous variables. Obviously, the singular perturbation approach is an inverse process to achieve our goal. However, we still can apply the singular perturbation approach to introduce the fast dynamics, so that the DAE comes back to the ODE without any reduction.

For general systems we formulate the problem as follows:

Given the differential-algebraic equations (DAE) of power system dynamics

$$\begin{cases} \dot{x} = f(x, y, p) & (2.36) \\ 0 = g(x, y, p) & (2.37) \end{cases}$$

Convert the DAE to the singularly perturbed ODE

$$\begin{cases} \dot{x} = f(x, y, p, \varepsilon) & (2.38) \\ \varepsilon \dot{y} = g^{FD}(x, y, p, \varepsilon) & (2.39) \end{cases}$$

Let us take an example to see why we want to do this.

2.3.1 A Simple Example of Using the Reduction Method

A DAE system is shown in (2.40a), (2.40b), and (2.40c):

$$\begin{cases} \dot{x} = -yx + 2p & (2.40a) \\ 0 = -y^2 + y\sqrt{1-x^2} - p & (2.40b) \\ x \in X \subset \Re^+,\ y \in Y \subset \Re^+,\ p \in P \subset \Re^+ & (2.40c) \end{cases}$$

where $p>0$ is a scalar parameter and assumed slowly changing. Due to the algebraic constraints (2.40b), we cannot directly integrate to find its dynamic response based on the DAE. The reduction method solves for fast variable y from (2.40b) and substitutes it in (2.40a), then integrate the remaining slow dynamics to obtain the trajectories of slow variable x or calculate eigenvalues through the reduced Jacobian matrix J_r in bifurcation analysis.

The equilibrium points of the above system satisfy

$$\begin{cases} 0 = -yx + 2p & (2.41a) \\ 0 = -y^2 + y\sqrt{1-x^2} - p & (2.41b) \end{cases}$$

From (2.41b) we have two solutions of y for a given p:

$$y = \frac{\sqrt{1-x^2} + \sqrt{1-x^2-4p}}{2} \tag{2.42a}$$

and

$$y = \frac{\sqrt{1-x^2} - \sqrt{1-x^2-4p}}{2} \tag{2.42b}$$

Substituting (2.42a) or (2.42b) in (2.41a), and letting

$$f_1(x, p) = -\left(\frac{\sqrt{1-x^2} + \sqrt{1-x^2-4p}}{2} \right) x + 2p \tag{2.43a}$$

and

$$f_2(x, p) = -\left(\frac{\sqrt{1-x^2} - \sqrt{1-x^2-4p}}{2} \right) x + 2p \tag{2.43b}$$

the system equilibrium points are the solutions of f_1=0 and f_2=0. Fig. 7 and Fig. 8 show the curves $f_1(x, p)$ and $f_2(x, p)$ for different values of p respectively. The points at which the curves cross the zero line are the system equilibrium points. We see that there are two equilibrium points for each value of p. When $0<p<0.125$, one of the two comes from f_1=0 and the other comes from f_2=0. When $0.125<p<0.1545$, both comes from f_1=0. When $p>0.1545$, no equilibrium point exists anymore.

Note, for this case, we can solve for y in terms of x explicitly. However, it is impossible to do that for most of nonlinear algebraic equations. For this simple example, we have two solutions of y and we have to deal with each of them respectively, which makes it more complicated in the procedure of analysis.

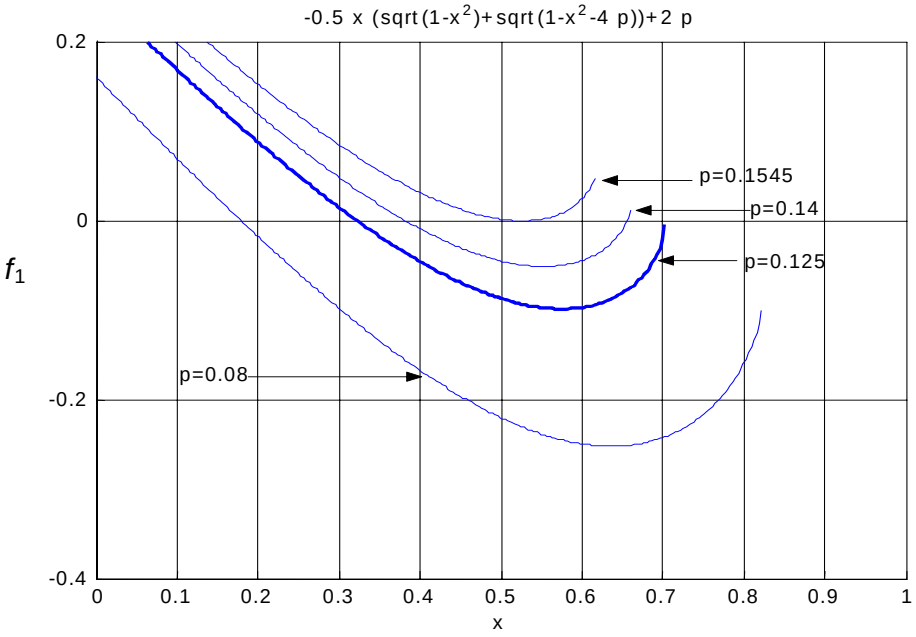

Fig. 7. The curves of $f_1(x, p)$ for different values of p.

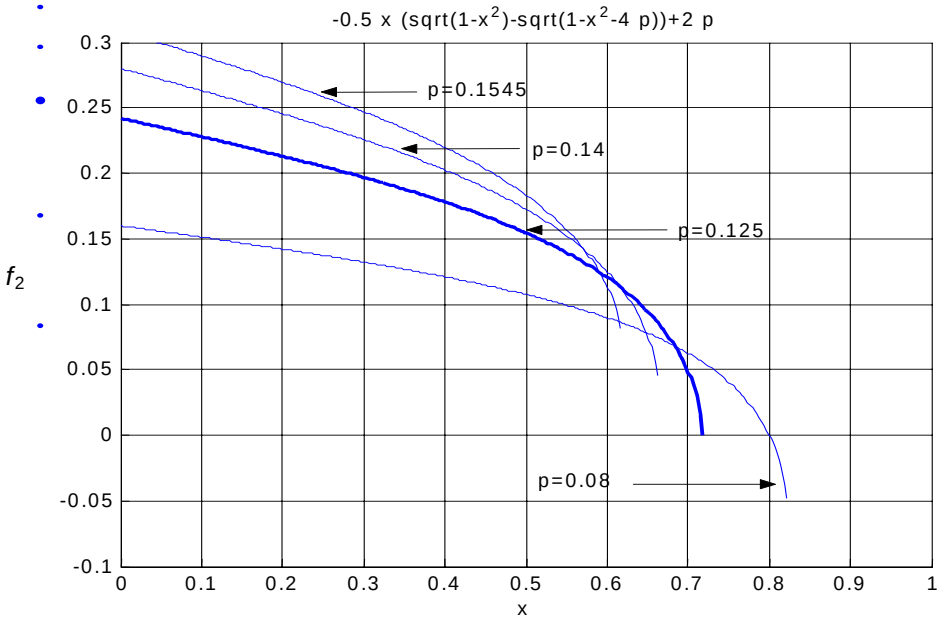

Fig. 8. The curves of $f_2(x, p)$ for different values of p.

Actually, these equilibrium points come from two differential equations in two reduced models. Substituting (2.42a) or (2.42b) in (2.40a), we obtain the reduced models in terms of slow dynamics accordingly:

$$\dot{x} = -\left[\frac{\sqrt{1-x^2}+\sqrt{1-x^2-4p}}{2}\right]x + 2p \tag{2.44a}$$

or

$$\dot{x} = -\left[\frac{\sqrt{1-x^2}-\sqrt{1-x^2-4p}}{2}\right]x + 2p \tag{2.44b}$$

The Jacobian matrices of the slow dynamics are as followings respectively:

$$J_r = -\left[\frac{\sqrt{1-x^2}+\sqrt{1-x^2-4p}}{2}\right] + \frac{1}{2}\left[\frac{1}{\sqrt{1-x^2}} + \frac{1}{\sqrt{1-x^2-4p}}\right]x^2 \tag{2.45a}$$

or

$$J_r = -\left[\frac{\sqrt{1-x^2}-\sqrt{1-x^2-4p}}{2}\right] + \frac{1}{2}\left[\frac{1}{\sqrt{1-x^2}} - \frac{1}{\sqrt{1-x^2-4p}}\right]x^2 \tag{2.45b}$$

As p varies, we can trace system equilibrium points and eigenvalues based on the reduced models above. TABLE I shows the corresponding equilibrium points and eigenvalues for different values of p:

TABLE I
EQUILIBRIUM POINTS AND EIGENVALUES OF THE DAE SYSTEM

P		C_+ component $\dot{x} = -\left[\frac{\sqrt{1-x^2}+\sqrt{1-x^2-4p}}{2}\right]x+2p$	C_- component $\dot{x} = -\left[\frac{\sqrt{1-x^2}-\sqrt{1-x^2-4p}}{2}\right]x+2p$
p=0.08		$x_e = 0.1789$ $y_e = 0.8944$ $\lambda = -0.8583$	$x_e = 0.8$ $y_e = 0.2$ $\lambda = -1.2667$
p=0.125 SIB	p=0.125$^-$	$x_e = 0.3162$ $y_e = 0.7906$ $\lambda = -0.6589$	$x_e = 0.7071$ $y_e = 0.3536$ $\lambda = -$inf
	p=0.125$^+$	$x_{e1} = 0.3162$ $y_{e1} = 0.7906$ $\lambda = -0.6589$ $x_{e2} = 0.7071$ $y_{e2} = 0.3536$ $\lambda =$ inf	No equilibrium point.
p=0.14		$x_{e1} = 0.3818$ $y_{e1} = 0.7333$ $\lambda = -0.5201$ $x_{e2} = 0.6559$ $y_{e2} = 0.4269$ $\lambda = 2.0322$	No equilibrium point.
p=0.1544		$x_{e1} = 0.5138$ $y_{e1} = 0.6010$ $\lambda = -0.0634$ $x_{e2} = 0.5375$ $y_{e2} = 0.5745$ $\lambda = 0.0694$	No equilibrium point.
p=0.1545 SNB		$x_{e1} = x_{e2} = 0.5257$ $y_{e1} = y_{e2} = 0.5878$ $\lambda = 0$	No equilibrium point.
p> 0.1545		No equilibrium point.	No equilibrium point.

We also present the *p*-*y* curve in Fig. 9. Along the *p*-*y* curve, the segment B-C corresponds to unstable equilibrium points while the others stable. This *p*-*y* curve is similar to the *P*-*V* curve in power system literature where *p* corresponds to *P*, the active power load; *y* corresponds to *V*, the load bus voltage.

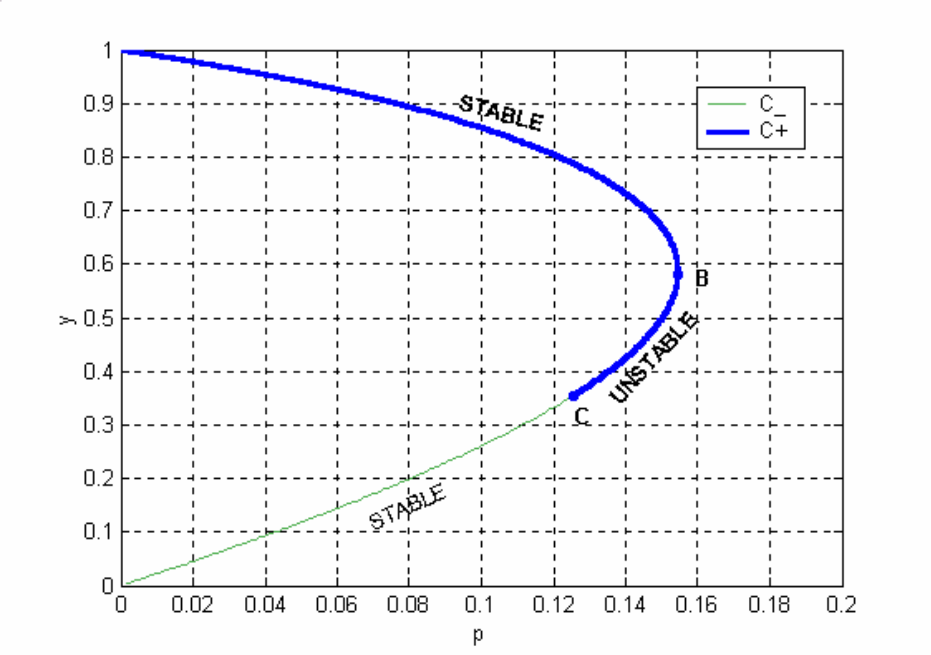

Fig. 9. The *p*-*y* curve of the DAE system. B: saddle-node bifurcation, C: singularity-induced bifurcation.

From TABLE I and Fig. 9, we have the following observations:

- *p*=0.125 corresponds to an SIB (point C in Fig. 9), where two equilibrium points, one to each side of C, have eigenvalues tending to infinity, but with an opposite sign.
- *p*=0.1545 corresponds to an SNB (point B in Fig. 9), where two equilibrium points, one stable and one unstable, coalesce and disappear with zero eigenvalue.

- When $0<p<0.1545$, there exist two equilibrium points of the system.
    - When $0<p<0.125$, two stable equilibrium points with two differential equations. One of the two equilibrium points comes from (2.43a) while the other one comes from (2.43b). Both eigenvalues are less than zero.
    - When $0.125<p<0.1545$, two equilibrium points with the differential equation (2.43a), one is stable, the other one unstable; and equation (2.43b) has no equilibrium point.
- When $p>0.1545$, no equilibrium points exist anymore.

In the dynamic state and instantaneous state space, i.e. *X, Y* space, the 2-dimensional constraint manifold, defined by (2.40b), is represented through a collection of contours shown in Fig. 10 with solid lines for different values of *p*. As already known, there is an SIB at point C as $p=0.125$. This SIB brings out the impasse surface (It is shown as a dashed curve marked IS in Fig. 10) that divides the constraint manifold by cut off on the tip into two components in the state space. The impasse curve is defined by the singularity of the fast dynamics:

$$g_y = -2y + \sqrt{1-x^2} = 0 \tag{2.46}$$

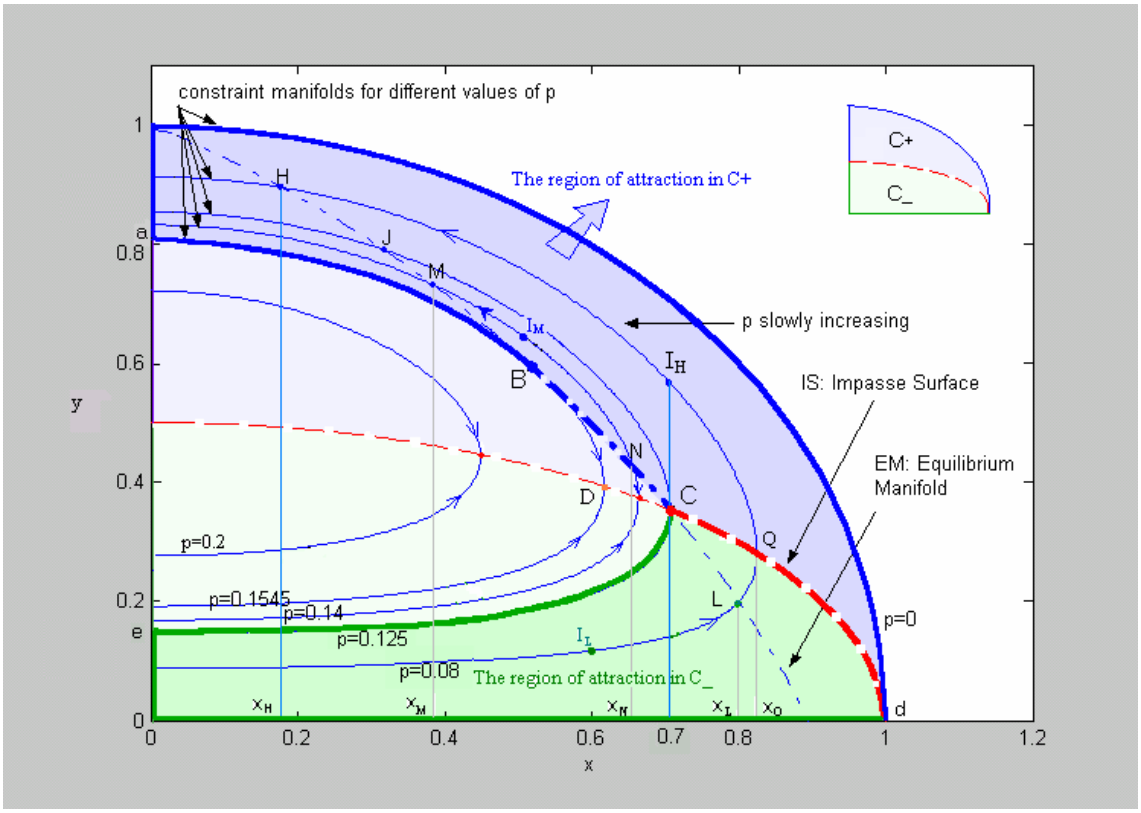

Fig. 10. Two components C_+ and C_ divided by IS. B: saddle-node bifurcation, C: singularity-induced bifurcation. The heavier lines represent the stability boundaries in C+ and C_ respectively.

The two components defined by (2.42a) and (2.42b) have their own dynamics defined by (2.44a) and (2.44b) respectively. Each dynamics has its own stability region in the state space. The two components are denoted here as C_+ and C_ shown in Fig. 10 respectively. In Fig. 5, we can also see that the singularity-induced bifurcation point C separates the *p*-*y* curve into the two components C_+ and C_.

The equilibrium points satisfy the conditions (2.41a) and (2.41b). From the two equations, we get the equilibrium manifold in *X*, *Y* space:

$$-y+\sqrt{1-x^2}-0.5x=0 \tag{2.47}$$

which is shown as a dash-dot curve marked EM in Fig. 10. Given $p>0$, the points at which the constraint manifold intersects the EM are the system equilibrium points for the specific value of p.

As seen in Fig. 10, when $p=0.125$, the equilibrium manifold EM together with the constraint manifold intersects the impasse surface IS at point C, which is the singularity-induced bifurcation. When $p=0.1545$, the equilibrium manifold EM tangents the constraint manifold at point B, which is a saddle-node bifurcation. The SNB and SIB are the critical points to determine the stability boundaries in parameter-state space.

Now, let us look into the region of attraction and the stability boundaries of the stable equilibrium points for each dynamics in C_+ and $C\_$ respectively. Here we just consider x, y, and p in $\Re^+$ space for simplicity.

On the C_+ *component*

- When $0<p<0.125$, there are two stable equilibrium points for each p that are defined, respectively, by two different stable dynamic equations in the two components C_+ and $C\_$, one to each side of the impasse surface IS (such as H in C_+ and L in $C\_$, see Fig. 10). Because system states cannot be defined on the impasse curve, the trajectories of the dynamics in C_+ cannot cross the IS into $C\_$, and vice verse. Hence, the segment d-C along IS lies on the stability boundaries of the stable equilibria in C_+.
- When $0.125<p<0.1545$, given p, we have two equilibrium points in C_+, one stable and one unstable (such as M and N as $p=0.14$, see Fig. 7). The unstable equilibrium point bounds the stability region of the stable one. As p varies

between 0.125 and 0.1545, the collection of the stable equilibria in C_+ consists of the segment B-J along the EM curve while the collection of the unstable equilibria in C_+ consists of the segment C-B. Thus, the C-B segment lies on the stability boundaries of the stable equilibria in C_+. As $0.125<p<0.1545$, the descending path from B in the direction of N is made up of unstable equilibria becoming more and more unstable with an eigenvalue approaching $+\infty$ at the SIB point C (see TABLE I).

- When p=0.1545, the saddle-node bifurcation occurs at point B. For the first order differential equation, B is a saddle-node in the sense that near B there exists a direction in the state space, along which trajectories behave as shown in Fig. 11, approaching the equilibrium from one side, and diverging on the other. In this case the system reaches the SNB by a gradual increase of *p*, the trajectory will depart from the equilibrium surface along the unstable manifold (the B-D curve in Fig. 10) of the SNB and it will end up on the impasse surface at point D which is not an equilibrium point. Similarly, if *p* is larger than 0.1545, all the trajectories will sink to the impasse curve along the corresponding constraint manifold (see the trajectory as p=0.2 in Fig. 10), and the system collapses in the sense that no equilibria exist anymore. Hence the B-a curve along the constraint manifold as p=0.1545 lies on the stability boundaries in C_+.

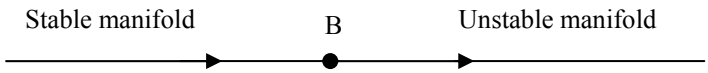

Fig. 11. Saddle-node B.

Therefore, the stability boundaries of the stable equilibrium point in C_+ are composed of the heavier curves d-C-B-a-1-d shown in Fig. 10.

On the C_ *component*

- When $0<p<0.125$, as already known above, the segment d-C lies on the stability boundaries in C_.
- When $p>0.125$, there is no equilibrium point in C_. Mathematically, if the initial point is in C_ as $p>0.125$, the trajectory will move along the corresponding constraint manifold in C_ and sink to the impasse surface (see the trajectories in C_ as $p>0.125$ in Fig. 10). Hence, the segment C-e along the constraint manifold as $p=0.125$ in C_ forms the rest of the stability boundaries of the stable equilibrium point in C_.

Therefore, the stability boundaries of the stable equilibria in C_ in X, Y, P space are composed of the heavier curves d-C-e-0-d shown in Fig. 10.

The region of attraction of the stable equilibrium points in C_+ is the open area bounded by the heavier line d-C-B-a-1-d in C_+. The stable equilibrium points in C_+ are composed of the segment B-M-J-H-1 along the EM curve. The region of attraction of the stable equilibrium points in C_+ is here in the sense that the states will return to a sable equilibrium point on the EM as long as the initial point of the system after subjected a

small disturbance is within the region. For example, suppose the system is operating at stable equilibrium point M as p=0.14 in C_+. The initial point after subjected a small disturbance is at point I_M. For the specific value of p, the region of attraction of the stable equilibrium point M is the curve along the corresponding constraint manifold above the unstable equilibrium point N in C_+. During the dynamic procedure, parameter p keeps constant under the assumption that p is slowly changing. The system states keep staying on the corresponding constraint manifold as p=0.14. Finally, the system trajectory will return to M since I_M is within the region of attraction of the stable equilibrium point M.

Likewise, the region of attraction of the stable equilibrium points in C_ is the open area bounded by the heavier line d-C-e-0-d in C_. For example, as p=0.08 we have a stable equilibrium point L in C_. If the initial point, upon clearing a small disturbance, is at point I_L within the region of attraction of the stable equilibrium point L, the system trajectory will return to L along the constraint manifold. The third region bounded by e-C-B-a-e contains no equilibria and all trajectories staying on constraint manifolds sink into the impasse curve (see the trajectories as p=0.2 in Fig. 10), where the system is not well defined and the event is unpredictable, resulting in the system collapse [17], [23].

As already known, the reduced models (2.44a) and (2.44b) represent the dynamics in terms of slow variable x defined in C_+ and C_ respectively. It is convenient to observe the stability boundary in X state space by simply project it to the x-axis in Fig. 10. For instance, as p=0.14, we have two equilibrium points in C_+ (see TABLE I and Fig. 10):

M: $(x_{e1}, y_{e1}) = (x_M, y_M) = (0.3818, 0.7333)$

and

$$\text{N:} \qquad (x_{e2}, y_{e2}) = (x_N, y_N) = (0.6559, 0.4269)$$

M is stable, and N is unstable. In X space, the stability boundary of the stable equilibrium x_{e1} (i.e. x_M in Fig. 10) is determined by the unstable equilibrium point x_{e2} (i.e. x_N in Fig. 10), which is illustrated in Fig. 12. Given x_0=0.5 (corresponding to initial point I_M in Fig. 10) within the region of attraction of the stable equilibrium x_M (=x_{e1}), the time response follows the path of (2.44a) and converges to the stable equilibrium point x_M (see Fig. 13).

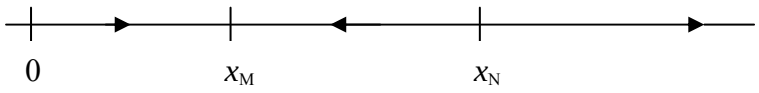

Fig. 12. Stability boundary in X space for p=0.14 in C_+.

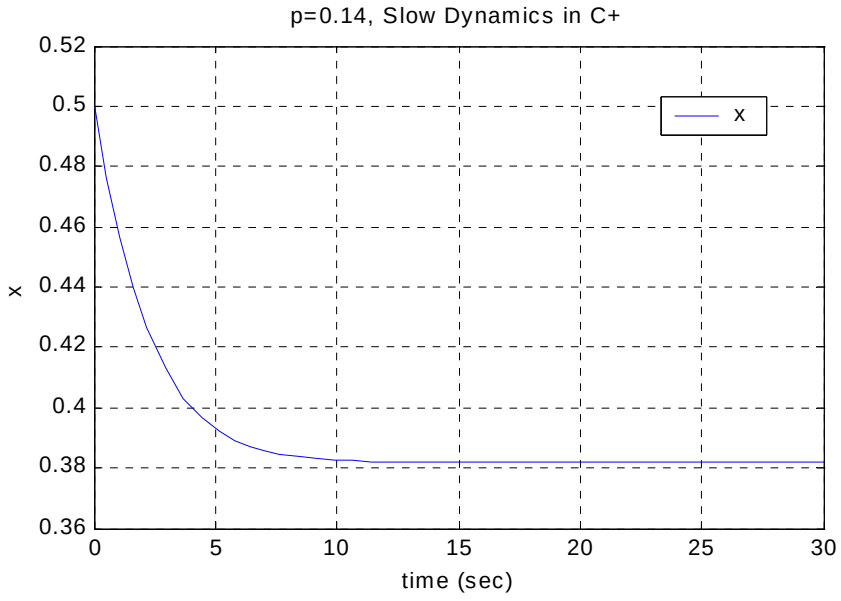

Fig. 13. Time response of (2.44a) converges to x_M=x_{e1}=0.3818. Initial x_0=0.5.

Similarly, as p=0.08, we have two stable equilibrium points H and L in C_+ and C_- respectively (see TABLE I and Fig. 10):

H: $(x_{e1}, y_{e1}) = (x_H, y_H) = (0.1789, 0.8944)$

and

L: $(x_{e2}, y_{e2}) = (x_L, y_L) = (0.8, 0.2)$

Since the impasse curve intersects the corresponding constraint manifold as p=0.08 at x_Q=0.8246, the stability boundary of the stable equilibrium point x_{e2} (i.e. x_L in Fig. 10) in C_- in X space is determined by x_Q (see Fig. 14). Note, the stability boundary of the stable equilibrium point x_{e1} (i.e. x_H in Fig. 10) in C_+ in X space is also determined by x_Q (see Fig. 15).

Given x_0=0.6 (corresponding to initial point I_L in Fig. 10) within the region of attraction of the stable equilibrium x_L (=x_{e2}), the time response follows the path of (2.44a) and converges to the stable equilibrium point x_L (see Fig. 16).

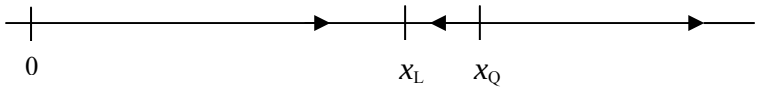

Fig. 14. Stability boundary in C_- in X space for p=0.08.

Fig. 15. Stability boundary in C_+ in X space for p=0.08.

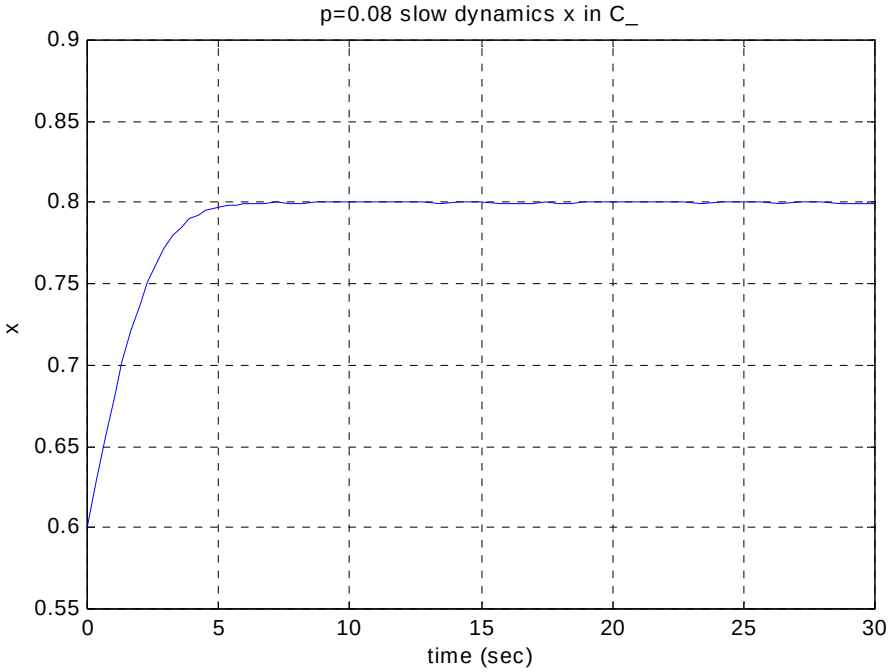

Fig. 16. Time response of (2.44b) converges to $x_L=x_{e2}=0.8$. Initial $x_0=0.6$.

As has been known, system trajectories that encounter impasse surface generally cannot continue because the system cannot be defined on the singular point [4]. From the engineering point of view, system can only work in one component with its dynamics defined in the component, such as (2.44a) defined in C_+ with wider region of attraction for this case. The other one is then physically meaningless. In real power systems, the equilibrium point in C_ is of too low bus voltage for operation. A system break up by selective protection will follow. Therefore, we always let the power system dynamics along the upper operating path in C_+. Fig. 17 shows such a case of p=0.08 (refer to TABLE I for the corresponding equilibrium points and eigenvalues) where the time response for x_0=0.7 (corresponding to initial point I_H in Fig. 10) converges to the stable equilibrium point x_H = 0.1789.

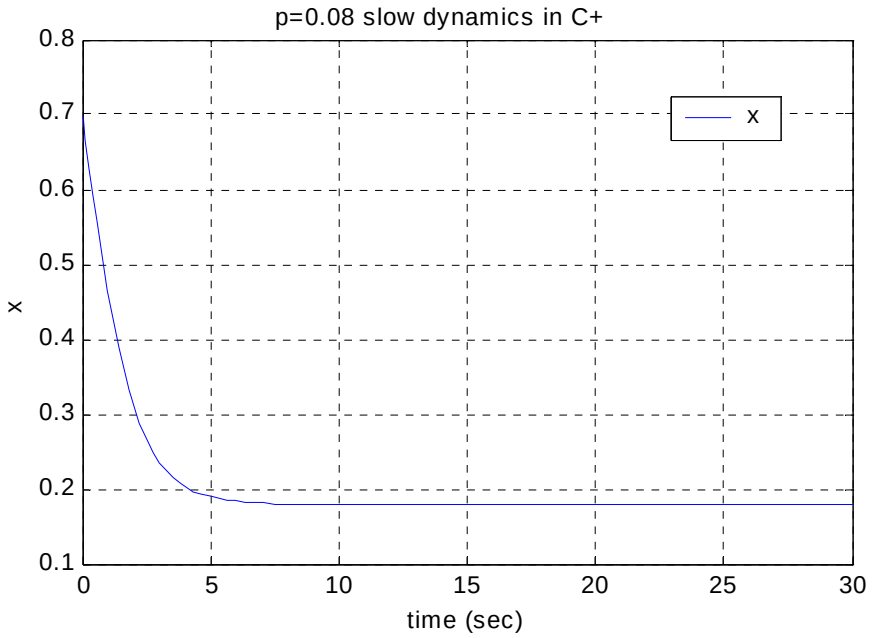

Fig. 17. Time response of (2.44a) converges to x_H=0.1789. Initial x_0 = 0.7.

From above we see that the procedure of the reduction method to analyze nonlinear DAE systems is quite complicated since we have to solve for *y* and deal with the two solutions of *y* and the two reduced slow dynamics of *x* respectively, which only gives local pictures of system behaviors. In the next section, we will discuss a singularly perturbed ODE form that well descries the original DAE system. Through the ODE, we avoid solving the nonlinear algebraic equations and directly perform integration without reduction process.

2.3.2 A Simple Example to Demonstrate Our New Singularly Perturbed ODE

Let us look into the singularly perturbed ODE. We put the original DAE here for convenience:

$$\begin{cases} \dot{x} = -yx + 2p & (2.48) \\ 0 = -y^2 + y\sqrt{1-x^2} - p & (2.49) \\ x \in X \subset \Re^+,\ y \in Y \subset \Re^+,\ p \in P \subset \Re^+ & (2.50) \end{cases}$$

Suppose the singularly perturbed ODE is expressed as below:

$$\begin{cases} \dot{x} = -yx + 2p & (2.51) \\ \varepsilon \dot{y} = -\left(\dfrac{-y^2 + y\sqrt{1-x^2} - p}{-2y + \sqrt{1-x^2}} \right) & (2.52) \end{cases}$$

where ε is the perturbation parameter and the Jacobian of algebraic equations is nonsingular, i.e.

$$g_y = -2y + \sqrt{1-x^2} \neq 0 \qquad (2.53)$$

The original DAE system is essentially approximated by a set of ODEs with an attractive manifold given by the algebraic constraint equations. The requirements of applying the singularly perturbed ODE will be discussed in the next section. The technique to convert a DAE to a singularly perturbed ODE will be introduced in chapter III. Here we just use the ODE and compare with the original DAE to analyze the system dynamics.

Once the singularly perturbed ODE is obtained, the time domain simulations or complex domain bifurcation analysis can be performed directly to this explicit state space form without any reductions.

The state x, y can be anywhere in the state space since there is no constraint manifold in the singularly perturbed ODE.

The equilibrium points of the ODE system follow the equations:

$$\begin{cases} 0 = -yx + 2p & (2.54) \\ 0 = -\left(\dfrac{-y^2 + y\sqrt{1-x^2} - p}{-2y + \sqrt{1-x^2}} \right) & (2.55) \end{cases}$$

Under the condition of (2.53), we get the same solutions of equilibrium points as the DAE:

$$\begin{cases} 0 = -yx + 2p & (2.56) \\ 0 = -y^2 + y\sqrt{1-x^2} - p & (2.57) \end{cases}$$

Thus in *X*, *Y* space, we have the same equilibrium manifold as DAE:

$$-y + \sqrt{1-x^2} - 0.5x = 0 \tag{2.58}$$

which is shown as a dash-dot curve marked EM in Fig. 18.

From (2.53) we also have the same impasse curve as the DAE defined by the singular surface:

$$g_y = -2y + \sqrt{1-x^2} = 0 \tag{2.59}$$

All the trajectories of the ODE system cannot cross the impasse surface. Like we mentioned in section 2.3.1, the impasse curve marked IS in Fig. 18 divides the state space into two components C_+ and C_ and the dynamics of the ODE system are defined in the two components. Note, due to (2.50), the ODE system is defined with the limitation of $0<x<1$, so that the two components are the open areas C_+ and C_ left to the line $x=1$. Since the algebraic equations are approximated by the fast dynamics (2.52), the instantaneous algebraic variable *y* becomes fast dynamic state *y*. Hence, the states *x* and *y* can be anywhere in the state space. The trajectories of the states *x*, *y* will follow the dynamics (2.51)-(2.52) and converge fast to the algebraic constraints in some local

neighborhood of the exact solution. This dynamic behavior of the ODE can be directly observed from phase portraits in phase plan, where the system dynamics are augmented in the state space through the recovery of fast dynamics. We will demonstrate it later on.

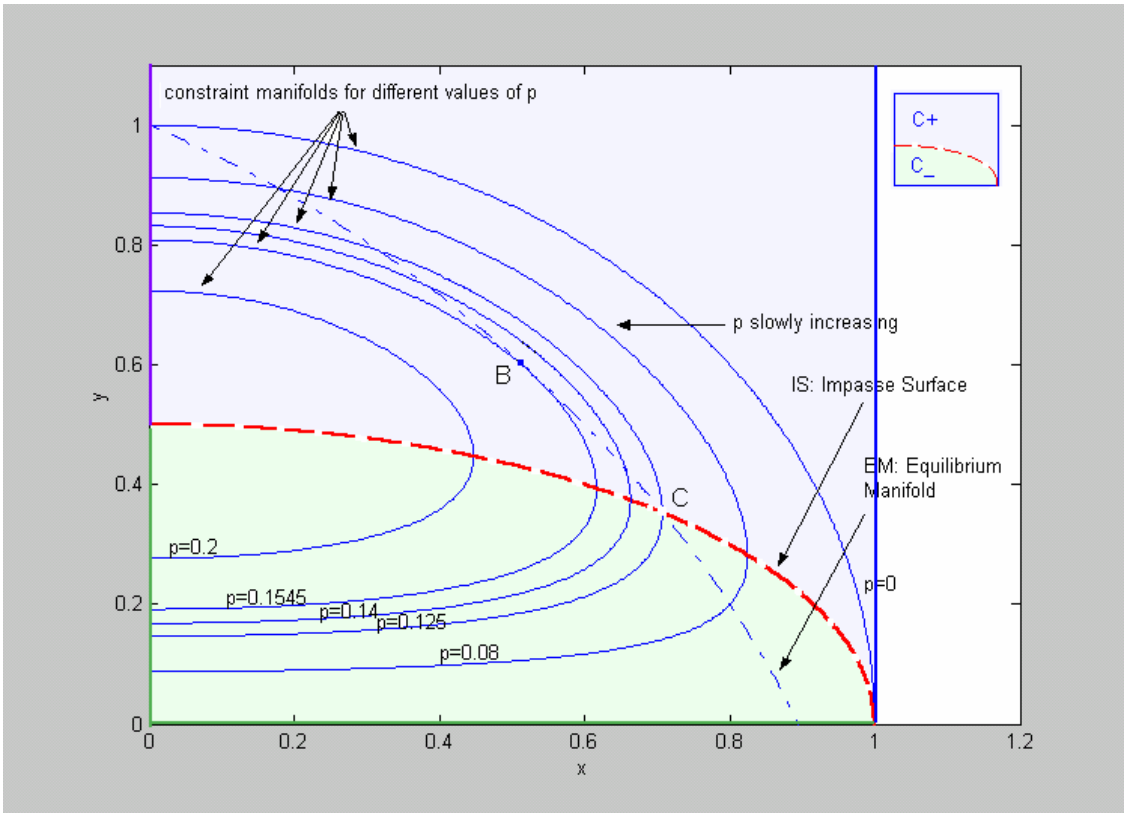

Fig. 18. The singularly perturbed ODE defined in components C_+ and C_. B: saddle-node bifurcation, C: singularity-induced bifurcation.

To analyze the dynamic behaviors of the ODE system, we solve for system equilibrium points for each given *p*. All the equilibrium points will be on the equilibrium manifold. The eigenvalues for each of the equilibrium points are calculated using the following unreduced Jacobian matrix:

$$J_u = \begin{bmatrix} -y & -x \\ -\frac{1}{\varepsilon}\frac{x}{(-2y+\sqrt{1-x^2})\sqrt{1-x^2}} & -\frac{1}{\varepsilon} \end{bmatrix} \tag{2.60}$$

where J_u is built in certain simplifications. We will discuss the system Jacobian of the ODE in detail in chapter III. As p varies, we trace system equilibrium points and eigenvalues based on (2.56), (2.57), and (2.60). TABLE II shows the corresponding equilibrium points and eigenvalues for different values of p.

Compared with the original DAE, the eigenvalue λ_1 of the unreduced Jacobian J_u is quite similar to the eigenvalue λ of the reduced Jacobian J_r. The negative λ_2 with large magnitude represents the very fast convergence of the fast dynamics.

We have already known that the original DAE has two bifurcations an SNB and an SIB. From TABLE II we see that the singularly perturbed ODE preserves the bifurcation properties of the original DAE system. The two bifurcations marked B and C respectively are shown in Fig. 18. In Fig. 19, we see that the singularity-induced bifurcation point C separates the *p*-*y* curve into the two components C_+ and C_-. Along the *p*-*y* curve, segment B-C corresponds to unstable equilibrium points while the others stable. This feature is just the same as the demonstrated in Fig. 9 for the DAE system in section 2.3.1.

TABLE II
EQUILIBRIUM POINTS AND EIGENVALUES OF THE ODE SYSTEM COMPARED WITH THE ORIGINAL DAE SYSTEM

p		Original DAE		Singularly perturbed ODE	
		C_+ component	C_- component	C_+ component	C_- component
p=0.08		x_e = 0.1789 y_e = 0.8944 λ = –0.8583	x_e = 0.8 y_e = 0.2 λ = –1.2667	x_e = 0.1789 y_e = 0.8944 λ_1 = –0.8583 λ_2 = –100000.0361	x_e = 0.8 y_e = 0.2 λ_1 = –1.2667 λ_2 = –99998.9333
p=0.125 SIB	p=0.125$^-$	x_e = 0.3162 y_e = 0.7906 λ = –0.6589	x_e = 0.7071 y_e = 0.3536 λ = –inf	x_e = 0.3162 y_e = 0.7906 λ_1 = –0.6588 λ_2 = –100000.1318	x_e = 0.7071 y_e = 0.3536 λ_1 = –inf λ_2 = –inf
	p=0.125$^+$	x_{e1} = 0.3162 y_{e1} = 0.7906 λ = –0.6589 x_{e2} = 0.7071 y_{e2} = 0.3536 λ = inf	No equilibrium point.	x_{e1} = 0.3162 y_{e1} = 0.7906 λ_1 = –0.6588 λ_2 = –100000.1317 x_{e2} = 0.7071 y_{e2} = 0.3536 λ_1 = inf λ_2 = –inf	No equilibrium point.
p=0.14		x_{e1} = 0.3818 y_{e1} = 0.7333 λ = –0.5201 x_{e2} = 0.6559 y_{e2} = 0.4269 λ = 2.0322	No equilibrium point.	x_{e1} = 0.3818 y_{e1} = 0.7333 λ_1 = –0.5201 λ_2 = –100000.2132 x_{e2} = 0.6559 y_{e2} = 0.4269 λ_1 = 2.0322 λ_2 = –100002.4590	No equilibrium point.
p=0.1545 SNB		$x_{e1} = x_{e2}$ =0.5257 $y_{e1} = y_{e2}$ =0.5878 λ = 0	No equilibrium point.	$x_{e1} = x_{e2}$ =0.5257 $y_{e1} = y_{e2}$ =0.5878 λ_1=0 λ_2= –100000.5878	No equilibrium point.
p> 0.1545		No equilibrium point.	No equilibrium point.	No equilibrium point.	No equilibrium point.

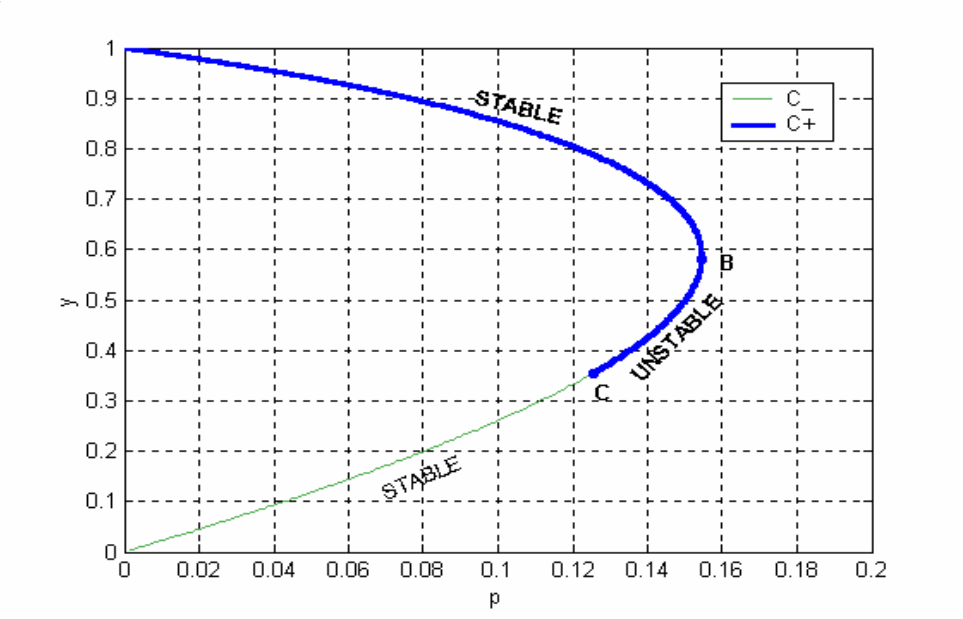

Fig. 19. The *p*-*y* curve of the ODE system. B: saddle-node bifurcation, C: singularity-induced bifurcation.

Now, let us look into the stability boundaries of the stable equilibrium point in the phase plane of the state space.

When $0<p<0.125$, we have two stable equilibrium points, say H and L as $p=0.08$, in C_+ and C_ respectively. See Fig. 20. Suppose the initial point is at point I_H in C_+ component. Upon clearing a disturbance, the system dynamics will converge very fast to the corresponding constraint manifold and return to the stable equilibrium point H along the constraint manifold. As $p=0.08$, the constraint manifold intersects the impasse curve at point Q. Thus, the vertical line ($x=0.8246$) passing though Q together with the impasse curve left to point Q consists of the stability boundaries of the stable equilibrium points H and L in C_+ and C_ respectively (marked heavier lines in Fig. 20). It is therefore, the region of attraction of the stable equilibrium point H in C_+ is the open area above the stability boundaries in C_+.

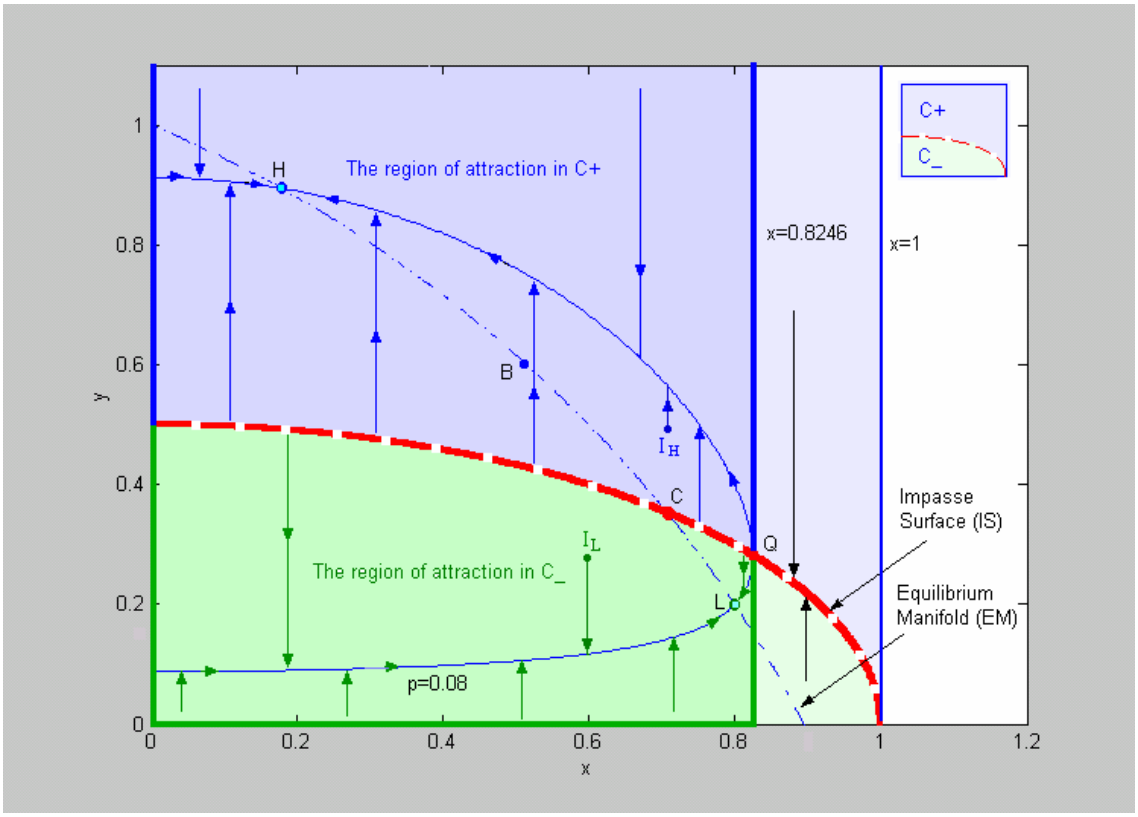

Fig. 20. Phase portrait as p=0.08. H: stable equilibrium point in C_+, L: stable equilibrium point in C_, B: saddle-node bifurcation, C: singularity-induced bifurcation.

Similarly, the region of attraction of the stable equilibrium point L in C_ is the open area below the stability boundaries in C_. This phase portrait also reflects the "slow down" of the fast dynamics through the small perturbation parameter ε (here $\varepsilon=10^{-5}$). If ε=0, the region of attraction will instantaneously shrink, in the y direction, to the constraint manifold that associates the DAE model. The trajectories for the initial point outside the region of attraction will sink to the impasse surface and the system collapses.

By projecting the phase plane to *x*-axis, we obtain the stability boundaries of the stable equilibrium point H and L in *X* space shown in Fig. 21 and Fig. 22 respectively, which are the same as the DAE model. Suppose the initial point is at I_H: $(x_0, y_0)=(0.7, 0.5)$ within the region of attraction of the stable equilibrium point H in C_+, the time responses of states *x*, *y* are shown in Fig. 23 where the trajectories approach to H. If the initial point is at I_L: $(x_0, y_0)=(0.6, 0.33)$ within the region of attraction of the stable equilibrium point L in C_, the time responses of states *x*, *y* are shown in Fig. 24 where the trajectories approach to L. All the trajectories are obtained by directly integrating the singularly perturbed ODE without substitutions and reductions like we did for the DAE in section 2.3.1.

Fig. 21. Stability boundary of the stable equilibrium point H in C_+ in *X* space as p=0.08.

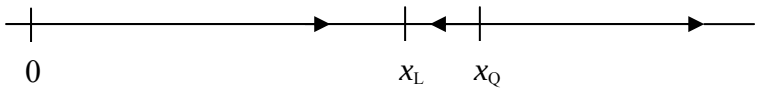

Fig. 22. Stability boundary of the stable equilibrium point L in C_ in *X* space as p=0.08.

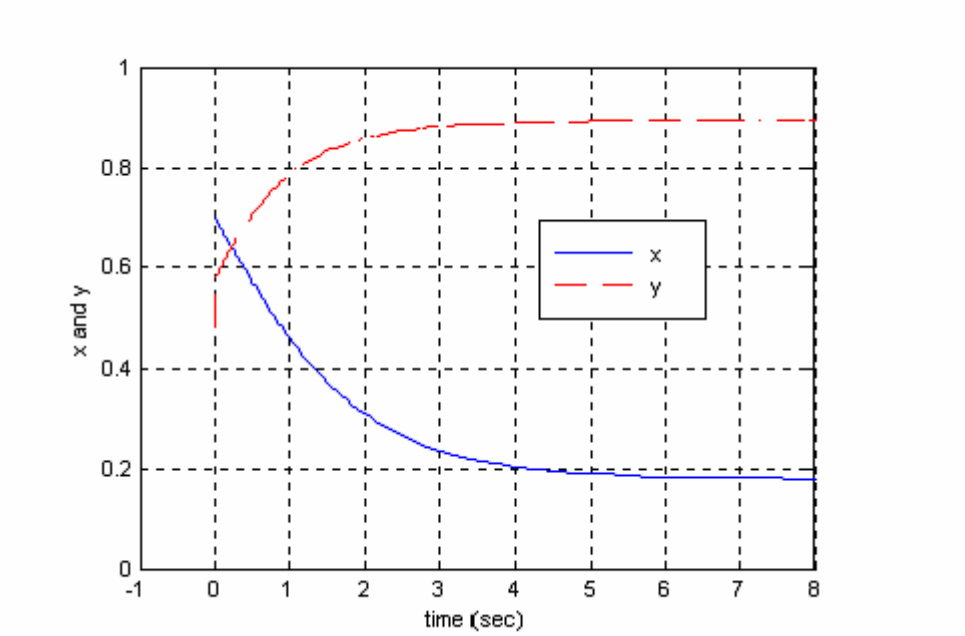

Fig. 23. Time response converges to H: (x_H, y_H)=(0.8944, 0.1789). Initial at I_H: (x_0, y_0)=(0.7, 0.5) in C_+ and p=0.08.

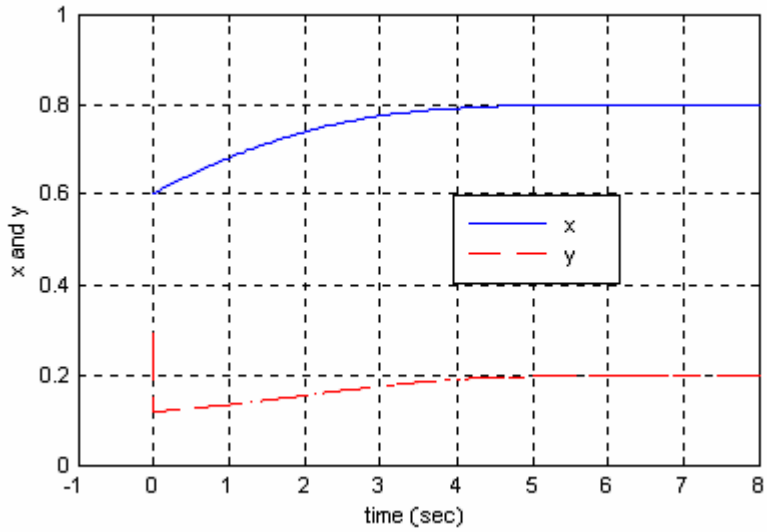

Fig. 24. Time response converges to L: (x_L, y_L)=(0.8, 0.2). Initial at I_L: (x_0, y_0)=(0.6, 0.33) in C_- and p=0.08.

As p increases slowly to p=0.125, the singularity-induced bifurcation point C occurs and no equilibrium point exists in C_. All the trajectories with initial point in C_ either sink to the impasse curve or to the SIB point C along the constraint manifold and eventually the system collapses. On the other hand, the system may work at the stable equilibrium point J in C_+ component as p=0.125. The phase portrait and the region of attraction of the stable equilibrium point J are shown in Fig. 25.

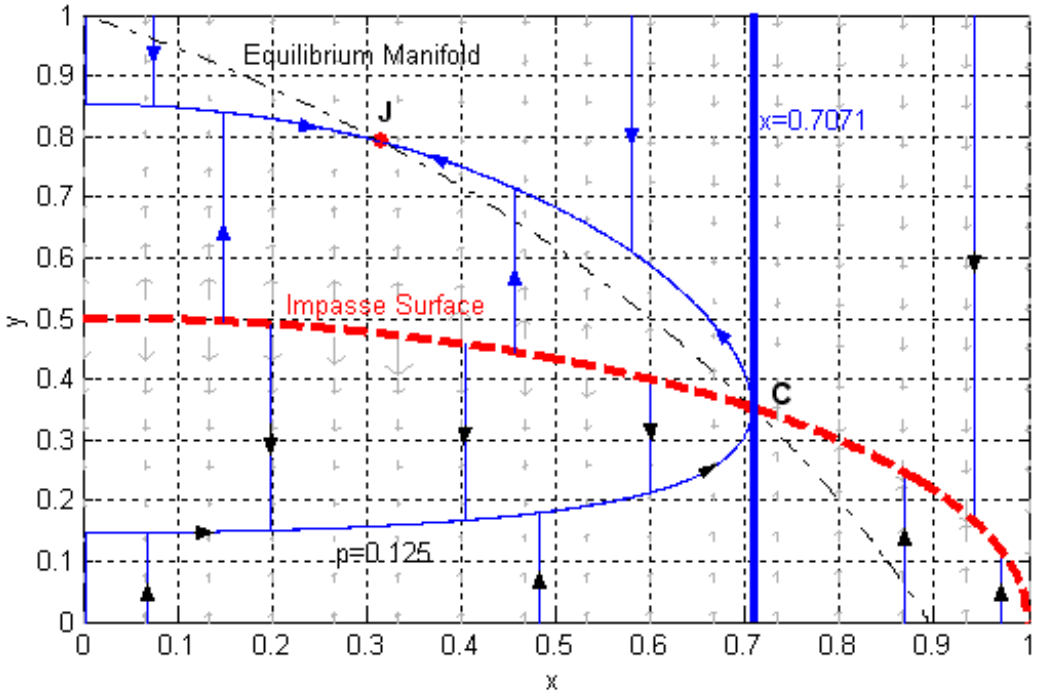

Fig. 25. Phase portrait as p=0.125. J: stable equilibrium point, C: singularity-induced bifurcation.

When 0.125<p<0.1545, we have two equilibrium points in C_+, one stable and one unstable, such as M and N as p=0.14 shown in Fig. 26. The unstable equilibrium point determines the stability boundaries of the stable one. In Fig. 26, the region of attraction

of the stable equilibrium point M is the open area above the impasse curve and left to line x=0.6559.

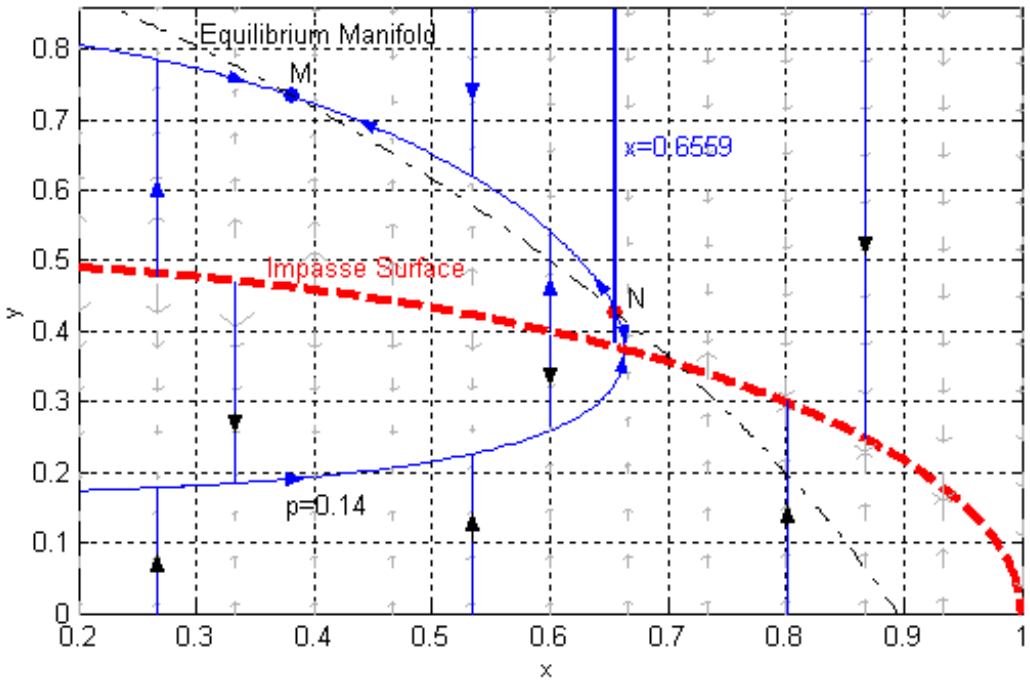

Fig. 26. Phase portrait as p=0.14. M: stable equilibrium point, N: unstable equilibrium point.

When p reaches 0.1545, a saddle-node bifurcation occurs at point B, where two equilibria meet and disappear with a zero eigenvalue. In this case the system reaches the SNB by a gradual increase of p, the trajectory will depart from the equilibrium surface along the B-D curve (see Fig. 27) and it will end up on the impasse surface at point D, which is not an equilibrium point. When p is lager than or equal to 0.1545, no stability region exists anymore. All the trajectories will sink to the impasse curve and the system get collapse.

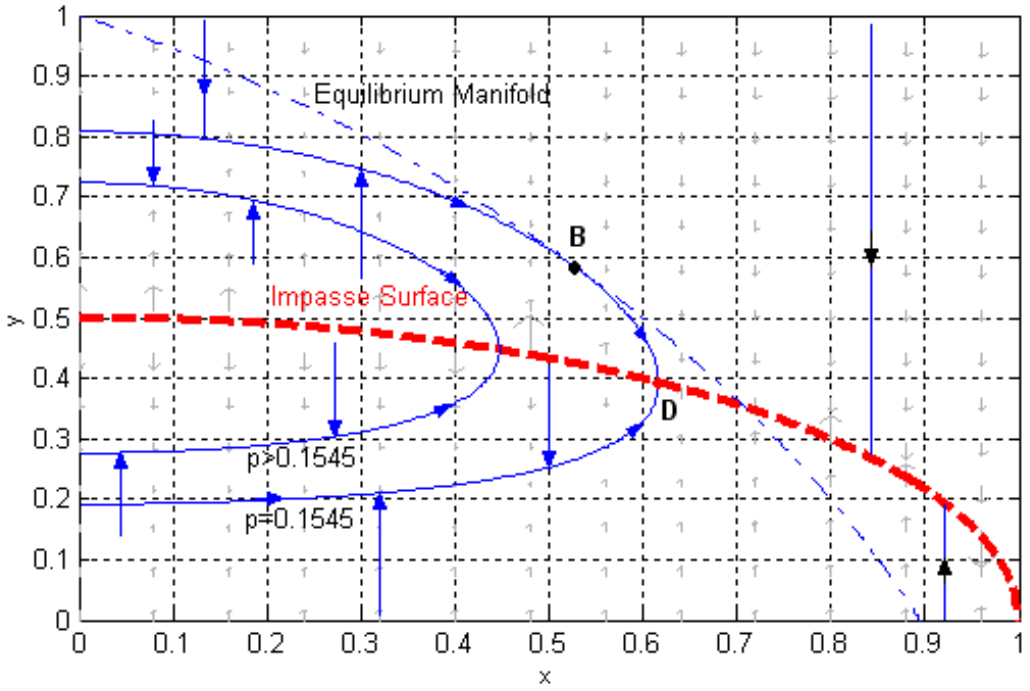

Fig. 27. Phase portrait as $p \geq 0.1545$. B: saddle-node bifurcation.

This example illustrates that we can observe time domain trajectories by directly integrating the singularly perturbed ODE without reduction computation. The ODE presented above preserves the bifurcation properties of the original DAE system. Since the fast dynamics is introduced, the instantaneous variable *y* becomes fast dynamic state *y*. Here the perturbation parameter ε plays the role to slow down the fast dynamics to observe. The slow state *x* and fast state *y* are no longer confined in the constraint manifold for all time. In other words, *x* and *y* can be anywhere in the state space. The components C_+ and C_ in which the ODE dynamics is defined are augmented with respect to fast state *y*. The stability region is therefore augmented in *X, Y* state space. Look into the phase portraits above, we see that the system dynamics converge very fast

to the algebraic constraints or to the impasse surface: when left to the tip point on the constraint manifold (at which the constraint manifold is cut off by the impasse curve), the impasse curve is kind of a source and all the trajectories depart from the impasse curve and converge very fast to the constraint manifold; when right to the tip point, the impasse curve is kind of a sink and all the trajectories move up or down to the impasse curve and eventually the system collapse in the sense that the system is not well defined on the impasse surface; when ε=0, the states instantaneously shrink, in the y direction, to the constraint manifolds of the DAE model. In conclusion, the augmentation of stability region is associated with fast state y. The stability boundaries and therefore the regions of attraction of stable equilibrium points in X state space keep the same as the original DAE system.

Through this example we see that the original DAE system is well descried by the singularly perturbed ODE. However, there still exist issues need to investigate: What are the requirements of using our singularly perturbed ODE? What are the complexities in the procedure of building fast dynamics? We will address these issues in detail in the coming sections.

2.4 The Requirements of Using the Singularly Perturbed ODE

To apply our new modeling approach, we need to investigate the requirements under which the DAE (2.36)-(2.37) can be successfully converted to the singularly perturbed ODE (2.38)-(2.39).

Three issues are discussed for our new singularly perturbed ODE:

2.4.1 $g^{FD}(x, y, p, \varepsilon)$ Describing the Fast Dynamics Is Not Necessary the Same As $g(x, y, p)$

For a valid approximation the fast dynamics must converge [13]; i.e., its eigenvalues must have negative real parts. However, this may not be true for the original algebraic constraints 0=*g*(*x, y, p*). For example, consider the original DAE system described by

$$\begin{cases} \dot{x} = -2x + y & (2.61a) \\ 0 = -x + y & (2.61b) \end{cases}$$

The reduced Jacobian matrix J_r is

$$J_r = -2 - (-1) = -1 \tag{2.62}$$

The eigenvalue of J_r is

$$eig(J_r) = -1 \tag{2.63}$$

The system is dynamic stable. But if we introduce the fast dynamics by simply setting $g^{FD}(x, y, p, \varepsilon) = g(x, y, p)$, we get

$$\begin{cases} \dot{x} = -2x + y & (2.64) \\ \varepsilon \dot{y} = -x + y & (2.65) \end{cases}$$

Then, the unreduced Jacobian matrix J_u is

$$J_u = \begin{bmatrix} -2 & 1 \\ -\frac{1}{\varepsilon} & \frac{1}{\varepsilon} \end{bmatrix} \tag{2.66}$$

The eigenvalues of J_u can be obtained by solve the following equation:

$$\begin{vmatrix} \lambda+2 & -1 \\ \frac{1}{\varepsilon} & \lambda-\frac{1}{\varepsilon} \end{vmatrix} = 0$$

They are

$$\lambda_1 = -1 + \frac{1}{2\varepsilon} + \sqrt{1+\frac{1}{4\varepsilon^2}} > 0 \tag{2.67}$$

$$\lambda_2 = -1 + \frac{1}{2\varepsilon} - \sqrt{1+\frac{1}{4\varepsilon^2}} < 0 \tag{2.68}$$

For any $\varepsilon>0$, we have eigenvalue $\lambda_1>0$. Therefore, the dynamic system (2.64)-(2.65) is unstable. It is clear that these two systems are totally different. The reason is that the fast dynamics $g^{FD}(x, y, p, \varepsilon)$ is diverging, since the Jacobian of the fast dynamics

$$\frac{1}{\varepsilon}\frac{\partial g^{FD}}{\partial y} = \frac{1}{\varepsilon}\frac{\partial g}{\partial y} = \frac{\partial(-x+y)}{\partial y} = \frac{1}{\varepsilon} \tag{2.69}$$

has a positive eigenvalue

$$eig(\frac{\partial g}{\partial y}) = \frac{1}{\varepsilon} > 0 \tag{2.70}$$

2.4.2 Fast Dynamics Has Eigenvalues with Larger Real Magnitude than That of Slow Dynamics

According to the fundamental linear control theory, the dynamic response depends on system characteristic root (i.e. eigenvalues) locations. If the roots are located far away from the imaging axis in the open left half complex plane, the converging response will be fast; and the slower it will be when approaching imaging axis.

Consider a standard second order linear system:

$$G(s) = \frac{\omega_n^2}{s^2 + 2\varsigma\omega_n + \omega_n^2} \tag{2.71}$$

The characteristic equation is

$$s^2 + 2\varsigma\omega_n + \omega_n^2 = 0 \tag{2.72}$$

The characteristic roots are

$$s_{1,2} = -\varsigma\omega_n \pm j\omega_n\sqrt{1-\varsigma^2} \tag{2.73}$$

The under damped response (ζ<1) to a unit step input, subject to zero initial condition, is given by

$$c(t) = 1 - \frac{e^{-\varsigma\omega_n t}}{\sqrt{1-\varsigma^2}}\sin(\omega_n t\sqrt{1-\varsigma^2} + \theta) \tag{2.74}$$

Where

$$\theta = \tan^{-1}\left(\frac{\sqrt{1-\varsigma^2}}{\varsigma}\right) \tag{2.75}$$

It is straightforward to see that the dynamic settle time mainly determined by $-\varsigma\omega_n$, the real part of the characteristic roots. For the second-order system, the response remains within 2 percent after 4 times constants, that is

$$t_s = \frac{4}{\varsigma\omega_n} \tag{2.76}$$

This suggests that the perturbation parameter ε need to be small enough to guarantee the fast dynamics converge fast. Again from above example (2.64)-(2.68), Let ε=10^{-5}, then

eigenvalue λ_1=99999.00001 in (2.67) corresponds to the fast dynamics, while λ_2=−1.00001 in (2.68) corresponds to the slow dynamics.

2.4.3 $g^{FD}(x, y, p, \varepsilon) = 0$ if and only if $g(x, y, p) = 0$

According to the singularly perturbed ODE, if fast dynamics $g^{FD}(x, y, p, \varepsilon)$ of (2.39) converges fast enough, then by taking ε=0 we can obtain a DAE system of the form (2.36)-(2.37). Since the singular perturbation approach is an inverse process of converting DAE to ODE, the ODE system (2.38)-(2.39) must approximate the original DAE system (2.36)-(2.37) well. Comparing these two systems, we know immediately that $g^{FD}(x, y, p, \varepsilon) = 0$ if and only if $g(x, y, p, \varepsilon) = 0$.

Now, according to above investigations, we have the following requirement to build the fast dynamics:

Fast dynamics converge fast to the algebraic constraints.

The singularly perturbed ODE is suitable for numerical integration to obtain time domain responses of dynamic systems. Based on the ODE, an unreduced Jacobian is also used in eigenvalue analysis, which should preserve the bifurcation properties of the original DAE systems. The detailed modeling technique will be described in chapter III.

2.5 Complexities of Building Fast Dynamics

From $\varepsilon \dot{y} = g^{FD}$ we know that the system will have different dynamic behaviors for different value of ε. When ε is close to zero, there are different instantaneous variable sequences can be employed to express the fast dynamics; In addition, g=0 implies $-g$=0. And also there exists a question of if the singular perturbation preserves the bifurcation properties of the original DAE system. These turn out complexities in building fast dynamics.

2.5.1 The Selection of ε

We introduce the perturbation parameter ε to slow down the fast dynamics. However, there are no explicit criteria to determine the value of ε need to ensure that the trajectories fast enough converge to the constraint manifolds. In addition, the error between the original DAE and the singularly perturbed ODE is related to ε. However, there is no explicit expression of bounding the approximation error [12]. In our applications, we select a small epsilon, say ε=10^{-5}. It shows that this ε is small enough to make the dynamic behavior of the singularly perturbed ODE system similar to the original DAE system.

2.5.2 The Different Sequences of Fast Dynamic States $\dot{y}$

Consider two ODEs with different sequences of fast dynamic states shown below

$$\begin{bmatrix} \dot{x}_1 \\ \varepsilon\dot{y}_1 \\ \varepsilon\dot{y}_2 \end{bmatrix} = \begin{bmatrix} -1 & 1 & 0 \\ 1 & -2 & 2 \\ 0 & 0 & -3 \end{bmatrix} \begin{bmatrix} x_1 \\ y_1 \\ y_2 \end{bmatrix} \tag{2.77}$$

$$\begin{bmatrix} \dot{x}_1 \\ \varepsilon\dot{y}_2 \\ \varepsilon\dot{y}_1 \end{bmatrix} = \begin{bmatrix} -1 & 1 & 0 \\ 1 & -2 & 2 \\ 0 & 0 & -3 \end{bmatrix} \begin{bmatrix} x_1 \\ y_1 \\ y_2 \end{bmatrix} \tag{2.78}$$

As ε is close to zero, both (2.77) and (2.78) are approximated by DAE (2.79). But the results of eigenvalue analysis shown in TABLE III are quite different.

$$\begin{bmatrix} \dot{x}_1 \\ 0 \\ 0 \end{bmatrix} = \begin{bmatrix} -1 & 1 & 0 \\ 1 & -2 & 2 \\ 0 & 0 & -3 \end{bmatrix} \begin{bmatrix} x_1 \\ y_1 \\ y_2 \end{bmatrix} \tag{2.79}$$

TABLE III
EIGENVALUES OF THE THREE SYSTEMS (ε=0.001)

ODE (2.77)	ODE (2.78)	DAE (2.79)
-0.5	-0.5	
-2000.5	3645.6	-0.5
-3000.0	-1646.1	

The ODE system (2.77) is stable that matches the DAE system (2.79), while the ODE system (2.78) unstable. The actual system Jacobian matrix of ODE (2.77) is

$$\begin{bmatrix} -1 & 1 & 0 \\ 0 & 0 & -3/\varepsilon \\ 1/\varepsilon & -2/\varepsilon & 2/\varepsilon \end{bmatrix} \tag{2.80}$$

Obviously the fast modes diverge because one of its eigenvalues $(1 \pm \sqrt{7})/\varepsilon$ is large than zero. The selection of the sequence depends on the fact that fast dynamics converge. So

we could not use the sequence shown in (2.77). For a system with m algebraic equations, there will be $m!$ different sequences to express the fast dynamics $\dot{y}$. However, there are no easy criteria to verify which one satisfies the fast convergence requirement.

2.5.3 The Sign Adjustment of Algebraic Equations

We noted that the algebraic equation $g(x,y,p)=0$ implies $-g(x,y,p)=0$. For one-dimensional algebraic constraint, the eigenvalue of J_r equals to J_r itself. Therefore, to guarantee the fast dynamics converge, one may just set $g^{FD}=g$ or $g^{FD}= -g$. There is an overhead in the decision to switch between these two options. For a DAE with m algebraic equations, there will be 2^m possibilities of different sign. However, there is no way to always guarantee fast modes converge by exhausting all the 2^m possibilities. TABLE IV shows that a 2-dimensional fast mode Jacobian has this scenario.

TABLE IV
SIGN ADJUSTMENT FOR m=2

Fast Mode Jacobian	$\begin{bmatrix}1 & 2\\ 2 & 1\end{bmatrix}$	$\begin{bmatrix}1 & 2\\ -2 & -1\end{bmatrix}$	$\begin{bmatrix}-1 & -2\\ -2 & -1\end{bmatrix}$	$\begin{bmatrix}-1 & -2\\ 2 & 1\end{bmatrix}$
Eigenvalues	-1 3	$1.7321j$ $-1.7321j$	-3 1	$1.7321j$ $-1.7321j$

2.5.4 The Singularly Perturbed ODE Is Not Necessary To Preserve the Bifurcation Properties of the Original DAE System

Fast convergence of fast dynamics is the requirement of using our new modeling approach to build fast dynamics. Singularly perturbed ODE form is valid only in the approximation sense. This implies that a singularly perturbed ODE is not necessary to preserve the bifurcation properties of the original DAE system, such as losing the significance of the singularity-induced bifurcation of the original DAE system. We will demonstrate this scenario in chapter III through a power system example.

2.6 Summary

In this chapter, we give fundamental insights on our modeling approaches. Through a simple example, a detailed dynamic analysis of using reduction method is demonstrated and compared with the singularly perturbed ODE. We can directly integrate the ODE to quickly view the local dynamic behaviors of the system through time responses. As has been seen, the singularly perturbed ODE makes it easier to analyze since we do not need solving the nonlinear algebraic equations. The bifurcation prosperities of the original DAE are preserved by the ODE.

We also discussed the requirements and the complexities of applying our new modeling approach. The requirement is

Fast dynamics converge fast to the algebraic constraints.

Therefore, we need new design methods to satisfy the fast convergence requirement to remodel a DAE by a singularly perturbed ODE, which is suitable for time domain simulation and preserve the bifurcation properties of the original DAE system.

CHAPTER III

THE TECHNIQUE OF PTE: PERTURB AND TAYLOR'S EXPANSION

In this chapter, we propose PTE technique to convert a DAE to a singularly perturbed ODE. Time domain simulation is then easily performed to this ODE to observe dynamic responses. A simplified unreduced Jacobian matrix of the ODE is introduced to perform eigenvalue analysis. Simulation results show that PTE technique satisfies the fast convergence requirement and preserves the bifurcation properties of the original DAE system. We will demonstrate PTE through a rudimentary power system example.

3.1 Describe Fast Dynamics by PTE

We convert DAE (3.1)-(3.2)

$$\begin{cases} \dot{x} = f(x, y, p) & (3.1) \\ 0 = g(x, y, p) & (3.2) \end{cases}$$

to a singularly perturbed ODE (3.3)-(3.4)

$$\begin{cases} \dot{x} = f(x, y, p, \varepsilon) & (3.3) \\ \varepsilon \dot{y} = g^{FD}(x, y, p, \varepsilon) & (3.4) \end{cases}$$

Fast dynamics described by g^{FD} needs to converge to the algebraic constraint g=0 fast to make our approximation meaningful. Under this condition, the simulation results obtained from the ODE will have similar behaviors as the original DAE. Since

$g(x, y, p) = 0$ is known, to get the fast dynamics of instantaneous variable *y*, we simply perturb it around the algebraic constraint by a small positive scalar ε,

$$0 = g(x, y + \varepsilon\dot{y}, p) \tag{3.5}$$

By Taylor's expansion we have

$$0 = g(x, y, p) + g_y(x, y, p)\varepsilon\dot{y} + o(\varepsilon) \tag{3.6}$$

Ignoring high order terms we have

$$g_y(x, y, p)\varepsilon\dot{y} = -g(x, y, p) \tag{3.7}$$

If g_y is nonsingular, then

$$\varepsilon\dot{y} = -g_y(x, y, p)^{-1} g(x, y, p) \tag{3.8}$$

Thus

$$\dot{y} = \frac{1}{\varepsilon} g^{FD} = -\frac{1}{\varepsilon} g_y^{-1} g \tag{3.9}$$

Equation (3.9) gives a generic expression of fast dynamics. Therefore, the singularly perturbed ODE obtained by PTE is as below:

$$\begin{cases} \dot{x} = f(x, y, p, \varepsilon) & (3.10) \\ \dot{y} = -\dfrac{1}{\varepsilon} g_y^{-1} g & (3.11) \end{cases}$$

The corresponding Jacobian matrix is given in (3.12):

$$J_u = \begin{bmatrix} f_x & f_y \\ \dfrac{1}{\varepsilon} g_x^{FD} & \dfrac{1}{\varepsilon} g_y^{FD} \end{bmatrix} \tag{3.12}$$

For eigenvalue analysis, we evaluate J_u at each equilibrium point. From (3.9) we have

$$g_y g^{FD} = -g \tag{3.13}$$

Taking the partial derivatives of the above equation in terms of x and y, we have

$$g_{yy} g^{FD} + g_y g_y^{FD} = -g_y \tag{3.14}$$

$$g_{yx} g^{FD} + g_y g_x^{FD} = -g_x \tag{3.15}$$

When g_y is nonsingular, substituting g^{FD} with $-g_y^{-1}g$ into above equations, we obtain

$$-g_{yy} g_y^{-1} g + g_y g_y^{FD} = -g_y \tag{3.16}$$

$$-g_{yx} g_y^{-1} g + g_y g_x^{FD} = -g_x \tag{3.17}$$

At each equilibrium point where g=0, the above two equations become

$$g_y^{FD} = -g_y^{-1} g_y = -I_{m\times m} \tag{3.18}$$

$$g_x^{FD} = -g_y^{-1} g_x \tag{3.19}$$

Or

$$\frac{1}{\varepsilon} g_y^{FD} = -\frac{1}{\varepsilon} I_{m\times m} \tag{3.20}$$

$$\frac{1}{\varepsilon} g_x^{FD} = -\frac{1}{\varepsilon} g_y^{-1} g_x \tag{3.21}$$

where I is an $m\times m$ identity matrix. Obviously, (3.20) assures that fast dynamics always converge fast since all its eigenvalues are $-1/\varepsilon$. Thus the unreduced Jacobian J_u becomes

$$J_u = \begin{bmatrix} f_x & f_y \\ -\frac{1}{\varepsilon} g_y^{-1} g_x & -\frac{1}{\varepsilon} I_{m\times m} \end{bmatrix} \tag{3.22}$$

For a large-scale power system, m can be huge, so J_u is a sparse matrix. Then we can use sparse techniques to compute its eigenvalues. On the contrary, a reduced Jacobian matrix

is not sparse and the solution efficiency is poor. For large power systems, the solution time is increased significantly [20].

In (3.22), it seems that we need to calculate the inverse of g_y to obtain J_u. But since g_y^{-1} is involved only in $-\frac{1}{\varepsilon} g_y^{-1} g_x$, an alternative way to avoid the inverse calculation is as below:

From

$$g_x^{FD} = -g_y^{-1} g_x \tag{3.23}$$

We have

$$g_y g_x^{FD} = -g_x \tag{3.24}$$

Here g_x, g_y are known at each operating point. So we can obtain the matrix multiplication of (3.23) by solving sparse linear equation of (3.24) under the assumption of a nonsingular g_y.

If g_y is singular, we cannot solve for g_x^{FD} uniquely or the solution may not exist. To handle this singularity, we apply perturbation technique again to get an approximate unique solution of g_x^{FD}. At this time we perturb g_y at the singular point by a small positive scalar ε_1, thus (3.7) becomes

$$(g_y \varepsilon + \varepsilon_1 I)\dot{y} = -g \tag{3.25}$$

Rewrite (3.25) by

$$\varepsilon(g_y + \mu I)\dot{y} = -g \tag{3.26}$$

where $\mu=\varepsilon_1/\varepsilon$. Therefore $(g_y+\mu I)$ is regularized by choosing $\mu=o(\varepsilon)$. We can solve for g_x^{FD} by

$$(g_y + \mu I) g_x^{FD} = -g_x \tag{3.27}$$

Hence, we can apply the PTE to describe a DAE by a singularly perturbed ODE. Dynamic analysis can then be performed to the ODE without reduction calculation. We can directly integrate slow dynamics $\dot{x}$ and fast dynamics $\dot{y}$ to obtain the time domain trajectories. To perform eigenvalue analysis, we calculate eigenvalues using the simplified unreduced Jacobian (3.22) and the bifurcation properties of the original DAE system are preserved by PTE.

Note that for the original DAE, the singularity of the Jacobian of algebraic equations (g_y=0) brings out the impasse surface lying on the constraint manifolds defined by (3.2). This impasse surface still exists in the singularly perturbed ODE. Under the assumption of g_y nonlinear, the equilibrium points of the ODE are the same as the DAE. We calculate system equilibrium points through the equations the same as the DAE:

$$\begin{cases} 0 = f(x, y, p) & (3.28) \\ 0 = g(x, y, p) & (3.29) \end{cases}$$

3.2 Case Study

In this section, we will apply PTE technique to a simple power system example. We will compare the simulation results with those of the reduction method. We focus on the dynamic voltage stability issues for this case.

3.2.1 Apply PTE to a Simple Power System

The simplified model shown in Fig. 28 retains the rudiments of power system voltage dynamics, i.e., generator, voltage control, transmission and load [17].

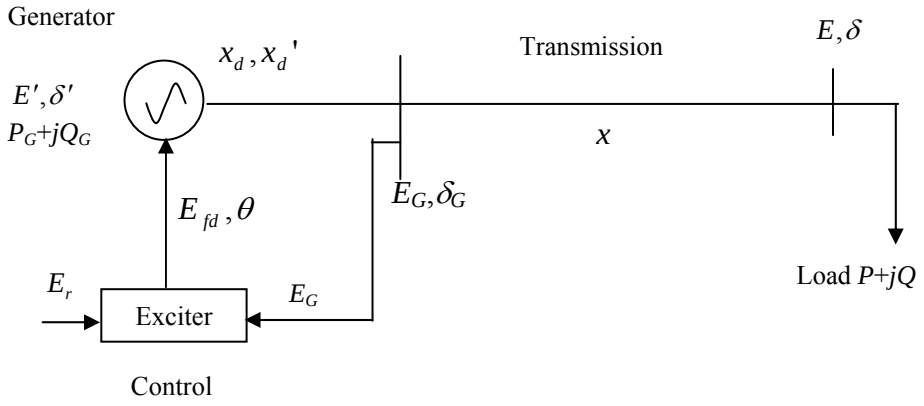

Fig. 28. A two-bus power system.

This simplified model includes a one-axis generator model and a first-degree simplification of the IEEE Type I excitation control [24] (refer to [17] for more details on the modeling assumptions). The following parameter dependent differential-algebraic equations describe the dynamics:

Dynamic Equations:

$$\dot{E}' = \frac{1}{T_{d0}'}\left[-\frac{x+x_d}{x'}E' + \frac{x_d - x_d'}{x'}\frac{E^2 + x'Q}{E'} + E_{fd}\right] \tag{3.30}$$

$$\dot{E}_{fd} = \frac{1}{T}\left[-(E_{fd} - E_{fd0}) - K\left(\frac{1}{E}\sqrt{(xP)^2 + (xQ + E^2)^2} - E_r\right)\right] \tag{3.31}$$

Algebraic Equation:

$$0 = E'^2 E^2 - (x'P)^2 - (x'Q + E^2)^2 \tag{3.32}$$

where E_r is the set-point voltage, E_{fd0} is the nominal field excitation, and T, K are control coefficients. The other notations are conventional. Equations (3.30)-(3.31) denote the dynamics of the excitation system, the slow state variable $x=\{E', E_{fd}\}$. Equation (3.32) denotes the power flow of the system, the fast variable $y=\{E\}$. The parameter p can be the load $p=\{P, Q\}$ which is treated as constant power load. This is a DAE model with two first-order differential equations (n=2) and one algebraic constraint (m=1). The unreduced Jacobian is a 3×3 dimensional matrix. We select $\varepsilon=10^{-5}$ and consider the system defined in $\Re^+$ space. The parameters of the system are:

$$T_{d0}' = 5,\ T = 1.5,\ E_{fd0} = 1.6,\ x_d = 1.2,\ x_d' = 0.2,$$
$$x = 0.1,\ x' = x + x_d',\ Q = 0.5P,\ K = 2.5,\ E_r = 1.0$$

Let

$$f_1(E', E_{fd}, E, P) = \frac{1}{T_{d0}'}\left[-\frac{x + x_d}{x'}E' + \frac{x_d - x_d'}{x'}\frac{E^2 + x'Q}{E'} + E_{fd}\right] \tag{3.33}$$

$$f_2(E', E_{fd}, E, P) = \frac{1}{T}\left\{-(E_{fd} - E_{fd0}) - K\left[\frac{1}{E}\sqrt{(xP)^2 + (xQ + E^2)^2} - E_r\right]\right\} \tag{3.34}$$

$$g(E', E_{fd}, E, P) = E'^2 E^2 - (x'P)^2 - (x'Q + E^2)^2 \tag{3.35}$$

The load flow constraint manifold is a vertical wall in E_{fd} for this case because E_{fd} does not appear in g. The singularity condition satisfies the following equation:

$$\frac{\partial g}{\partial E} = 2E'^2 E - 4(x'Q + E^2)E = 0 \tag{3.36}$$

which brings out the impasse surface defined by (3.36). The impasse surface separates

the load flow manifolds into two components C_+ and $C\_$ in the parameter-state space. Each component has its own dynamics. Look into the DAE, we see that we can solve for E^2 from (3.35) and substitute it in (3.33) and (3.34) to get reduced models in the each of the components. However, at this time, we simply apply PTE technique to avoid the reductions. The dynamic behavior of the singularly perturbed ODE will match that of the DAE system. We will observe the time responses and trace the bifurcations directly through the singularly perturbed ODE. All the results will be compared with the original DAE system.

(1) Time Domain Simulation

Once PTE is applied to the DAE, we have the singularly perturbed ODE as below:

$$\dot{E}' = \frac{1}{T_{d0}'}\left[-\frac{x+x_d}{x'}E' + \frac{x_d - x_d'}{x'}\frac{E^2 + x'Q}{E'} + E_{fd}\right] \tag{3.37}$$

$$\dot{E}_{fd} = \frac{1}{T}\left[-(E_{fd} - E_{fd0}) - K\left(\frac{1}{E}\sqrt{(xP)^2 + (xQ + E^2)^2} - E_r\right)\right] \tag{3.38}$$

$$\dot{E} = -\frac{1}{\varepsilon}\left[\frac{E'^2 E^2 - (x'P)^2 - (x'Q + E^2)^2}{2EE'^2 - 2(x'Q + E^2)E}\right] \tag{3.39}$$

As concluded in chapter II, the fast dynamics (3.39) converge fast to the load flow manifold (3.32). The stability regions in the slow state *E'*, E_{fd} space are the same as the DAE system. Upon a clearing of a disturbance, we can observe the time responses of the system dynamics starting from an initial point in the state space by directly

integrating the ODE (3.37), (3.38), and (3.39). During the dynamic procedure, the constant power load is fixed under the assumption that P is slowly changing.

(2) Eigenvalue Analysis

The unreduced Jacobian matrix of the singularly perturbed ODE is

$$J_u = \begin{bmatrix} f_x & f_y \\ -\frac{1}{\varepsilon} g_x^{FD} & -\frac{1}{\varepsilon} \end{bmatrix} \tag{3.40}$$

As the constant power load P slowly changes, we trace the system equilibrium points and calculate eigenvalues of J_u at each of the equilibrium points. For this case, we have

$$f_x = \begin{bmatrix} \frac{\partial f_1}{\partial E'} & \frac{\partial f_1}{\partial E_{fd}} \\ \frac{\partial f_2}{\partial E'} & \frac{\partial f_2}{\partial E_{fd}} \end{bmatrix} \tag{3.41}$$

$$f_y = \begin{bmatrix} \frac{\partial f_1}{\partial E} \\ \frac{\partial f_2}{\partial E} \end{bmatrix} \tag{3.42}$$

The g_x^{FD} in J_u is calculated by solving the following linear equation:

$$g_y g_x^{FD} = -g_x \tag{3.43}$$

where

$$g_x = \begin{bmatrix} \frac{\partial g}{\partial E'} & \frac{\partial g}{\partial E_{fd}} \end{bmatrix} \tag{3.44}$$

$$g_y = \begin{bmatrix} \frac{\partial g}{\partial E} \end{bmatrix} \tag{3.45}$$

We will see that the PTE technique preserves the bifurcations of the original DAE system.

3.2.2 Simulation Results

Starting with a base case, let the load active power P slowly increase, the associated P-V curve is shown in Fig. 29.

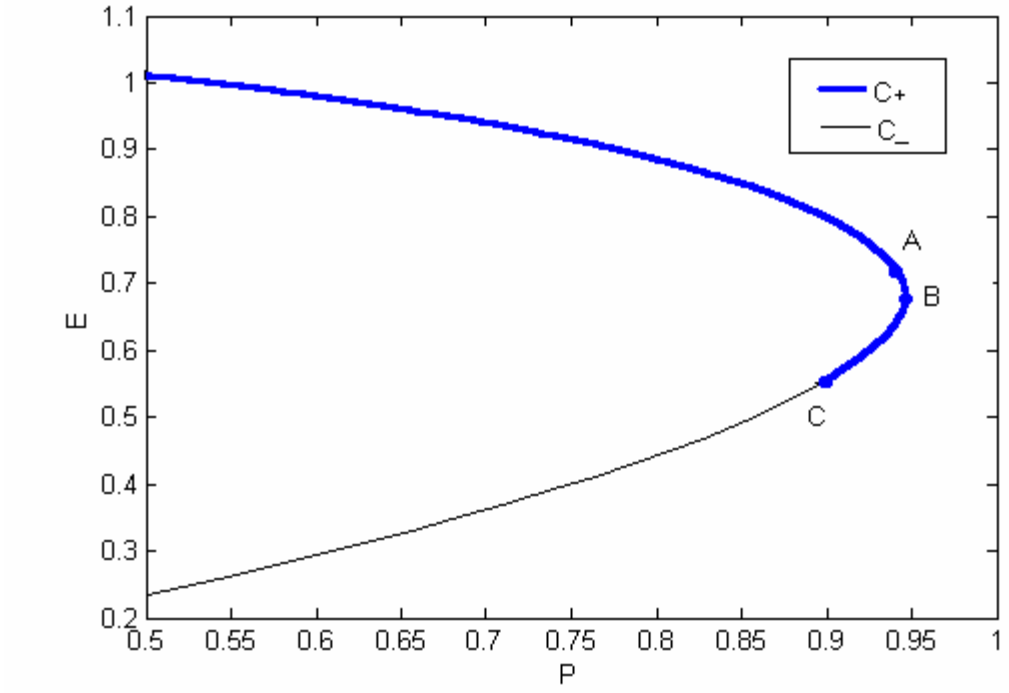

Fig. 29. The P-V curve. A: Hopf bifurcation, B: saddle-node bifurcation, C: singularity-induced bifurcation.

As P changes, we obtain three bifurcation points A, B, and C based on the singularly perturbed ODE, which are the same as the original DAE form. The three bifurcation points are: Hopf bifurcation A, saddle-node bifurcation B and singularity-

induced bifurcation C. The singularity-induced bifurcation point C (as P=0.89) divides the P-V curve into two components. The C_+ component corresponds to the P-V curve above point C (thick line in Fig. 29) while the C_ component corresponds to the P-V curve below point C (thin line in Fig. 29).

Let the constant power load P slowly increases from P>0. We have two equilibrium points in this case. As P<0.89, one is in C_+, and one is in C_. As 0.89<P<0.9424, both equilibrium points are in C_+. As P>0.9424, no equilibrium point exists anymore.

We observe the three bifurcations in detail in TABLE V. Some associated time domain trajectories of slow dynamics are shown in Fig. 30 through Fig. 32.

TABLE V shows that a pair of conjugate complex eigenvalues crosses the imaging axis of complex plane from left to right. There exists a Hopf bifurcation point between P=0.9358 and P=0.9359, which occurs on the feasibility boundary of the equilibrium of high load bus voltages. It has been shown to be sub-critical [1], [21], i.e., the limit cycle corresponding to the exciter states is unstable. However, load flow solution still exists. In voltage collapse studies, it was shown that the exciter mode might go unstable first. The local transients near the Hopf bifurcation can be demonstrated as shown in Fig. 30 through Fig. 33. As P=0.92, starting from the initial point showing in Fig. 30, Fig. 31, and Fig. 32, the time responses converge to the stable equilibrium point in an oscillatory fashion. In Fig. 33, As P=0.94, the trajectories diverge away from the unstable equilibrium in an oscillatory fashion.

TABLE V
HOPF BIFURCATION POINT A

A (HB)		Eigenvalues	
		P=0.9358	P=0.9359
C_+	Equilibrium point	E' = 1.0040 E_{fd} = 2.0678 E = 0.7397	E' = 1.0038 E_{fd} = 2.0686 E = 0.7394
	eigJ_r	–0.0005+j0.3838 –0.0005–j0.3838	0.0007+j0.3827 0.0007–j0.3827
	eigJ_u	–0.0005+j0.3838 –0.0005–j0.3838 -100001.8655	0.0007+j0.3827 0.0007–j0.3827 -100001.8676
	Equilibrium point	E' = 0.9651 E_{fd} = 2.2781 E = 0.6410	E' = 0.9652 E_{fd} = 2.2773 E = 0.6414
	eigJ_r	1.4787 –0.2046	1.4678 –0.2037
	eigJ_u	1.4787 –0.2046 –100003.1427	1.4678 –0.2037 –100003.1327
C_-	No equilibrium points		

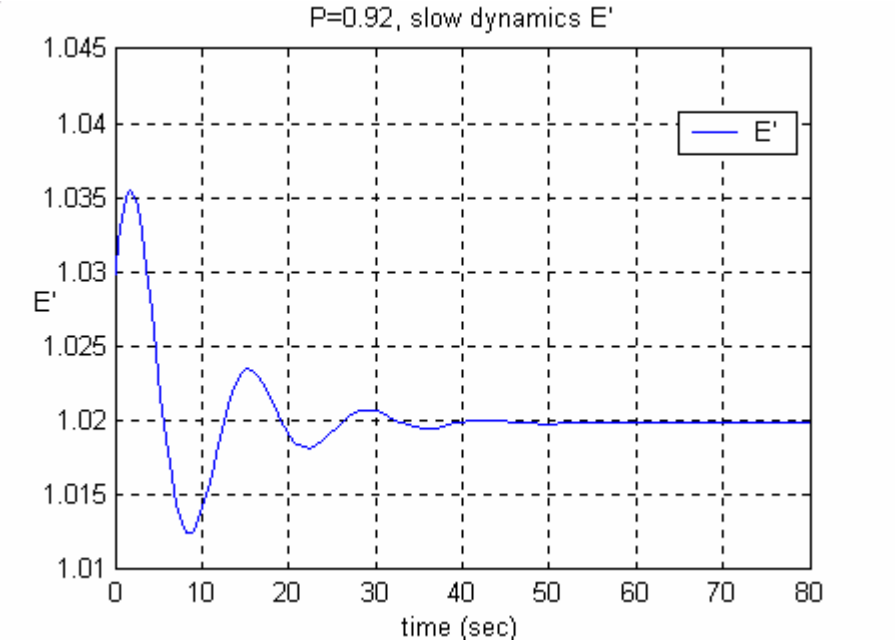

Fig. 30. Time response of *E'* converges to the stable equilibrium *E'*=1.0199. Initial at *E'*(0)=1.03.

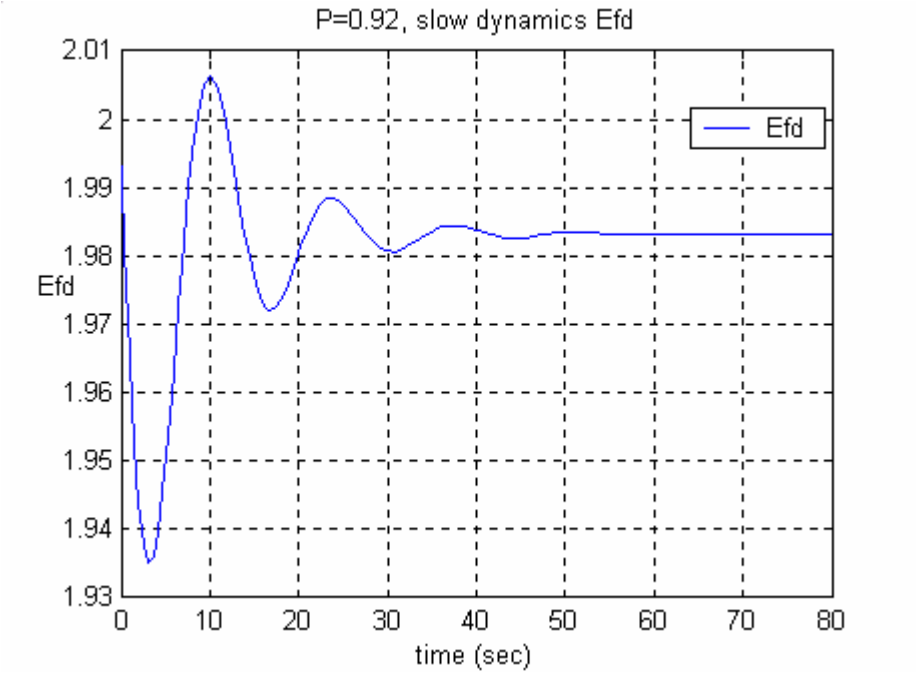

Fig. 31. Time response of E_{fd} converges to the stable equilibrium E_{fd}=1.983. Iinitial at $E_{fd}(0)$=1.993.

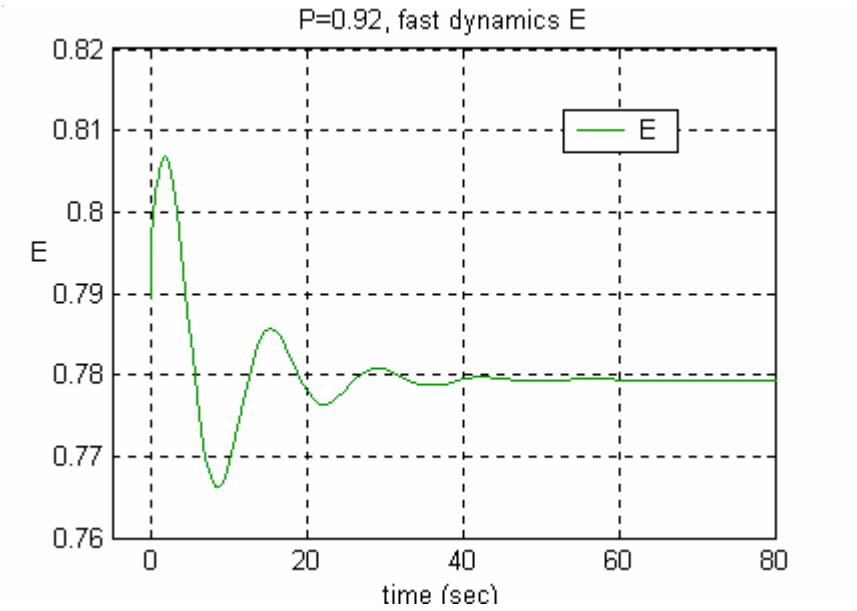

Fig. 32. Time response of E converges to the stable equilibrium E=0.799. Iinitial at $E(0)$=0.79.

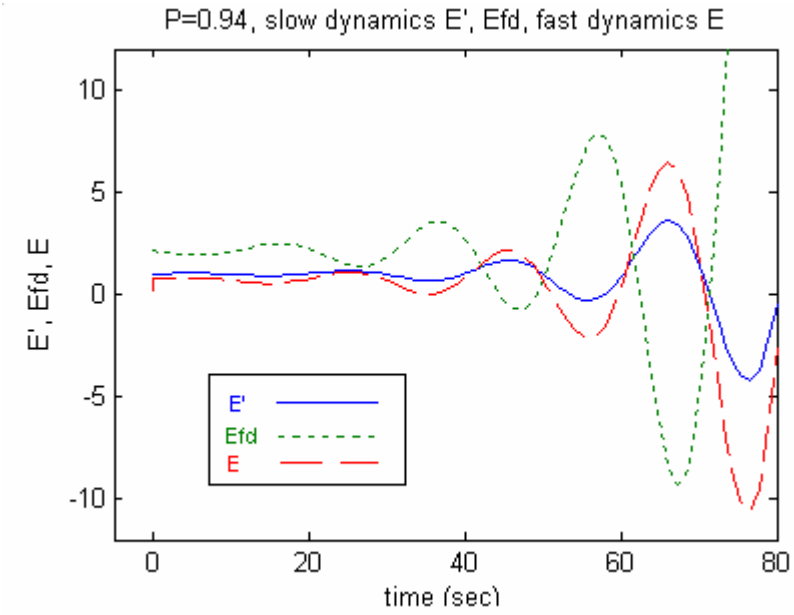

Fig. 33. Time responses of E', E_{fd}, and E diverge away from the unstable equilibrium E'=0.996, E_{fd} = 2.018, E=0.72. Initial at $E'(0)$=0.997, $E_{fd}(0)$=2.019, $E(0)$=0.3.

TABLE VI
SADDLE-NODE BIFURCATION POINT B

B (SNB)		Eigenvalues	
		P=0.9424	P>0.9424
C_+	Equilibrium point	E' = 0.9853 E_{fd} = 2.1678 E = 0. 6927	No equilibrium points
	eigJ_r	0. 3771 0.0177	
	eigJ_u	0. 3771 0.0177 –100002.2064	
	Equilibrium point	E' = 0. 9841 E_{fd} = 2.1753 E = 0. 6893	
	eigJ_r	0. 4483 –0.0152	
	eigJ_u	0. 4483 –0.0152 –100002.3619	
C_-	No equilibrium points		

TABLE VI shows that a saddle and an unstable node crosses and then disappear as P slightly large than 0.9424. Accordingly, there is a saddle-node bifurcation point B. In Fig. 34 we see that the time responses monotonically diverge as P approaches the collapse point. This is consistent with the results shown in TABLE VI that all eigenvalues are real numbers when approaching P=0.9424. Two equilibrium paths, a higher bus voltage path and a lower bus voltage path both in C_+, coalesce and disappear

at the saddle-node bifurcation B on the tip of the *P-V* curve. After point B (*P*>0.9424), no power flow solutions exist anymore and results in voltage collapse [19].

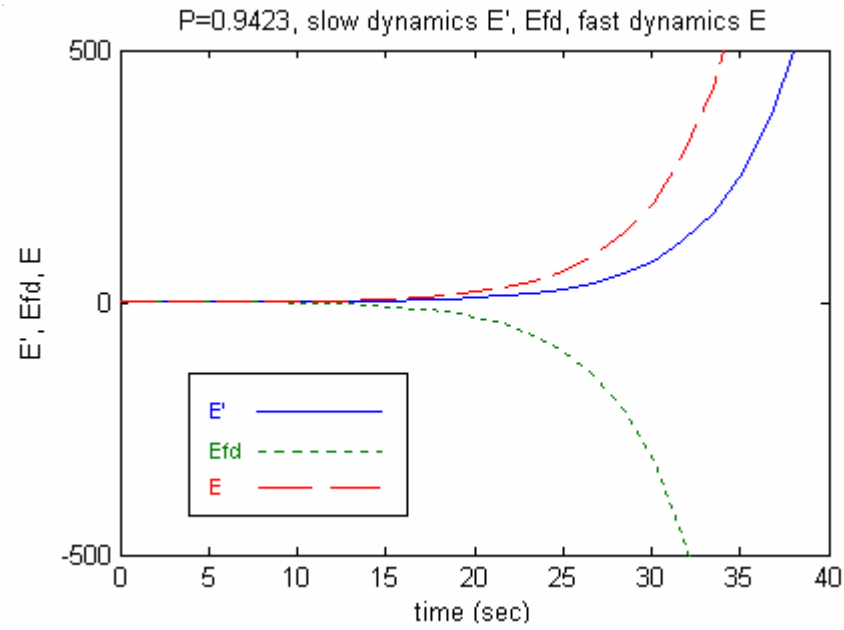

Fig. 34. Time responses of *E'*, E_{fd} and *E* monotonically diverge. Initial at *E'*(0)=0.9874, E_{fd}(0)=2.1569, *E*(0)=0.6989.

TABLE VII and Fig. 35 show that a real eigenvalue changes sign from minus infinity to plus infinity at point C. There is a singularity-induced bifurcation point between *P*=0.8898 and *P*=0.8900. This SIB point cannot be crossed by the trajectories of the system dynamics. Mathematically, all the trajectories in the C_ component converge to the singular point and causing the system to collapse. As P=0.89, the equilibrium point in C_+ component is a stable focus with its region of attraction in the C_+ component [19]. The time responses for the initial point in the C_+ component are shown in Fig. 36, Fig. 37, and Fig. 38.

TABLE VII
SINGULARITY-INDUCED BIFURCATION POINT C

C (SIB)		Eigenvalues	
		P=0.8898	P=0.89
C_+	Equilibrium point	E' = 1.0381 E_{fd} = 1.8877 E = 0. 8243	E' = 1.0380 E_{fd} = 1.8879 E = 0. 8242
	eigJ_r	–0.1923+j 0.4989 –0.1923–j 0.4989	–0.1919+j 0.4988 –0.1919–j 0.4988
	eigJ_u	–0.1923+j 0.4989 –0.1923–j 0.4989 –100001.4819	–0.1919+j 0.4988 –0.1919–j 0.4988 –100001.4828
	Equilibrium point		E' = 0. 9295 E_{fd} = 2.4782 E = 0. 5464
	eigJ_r		1457.7860 –0. 3481
	eigJ_u		1437.1113 –0. 3480 –101438.6300
C_-	Equilibrium point	E' = 0. 9294 E_{fd} = 2.4786 E = 0. 5463	No equilibrium points
	eigJ_r	–1484. 0548 –0. 3482	
	eigJ_u	–1506.7344 –0. 3482 –100000.7838	

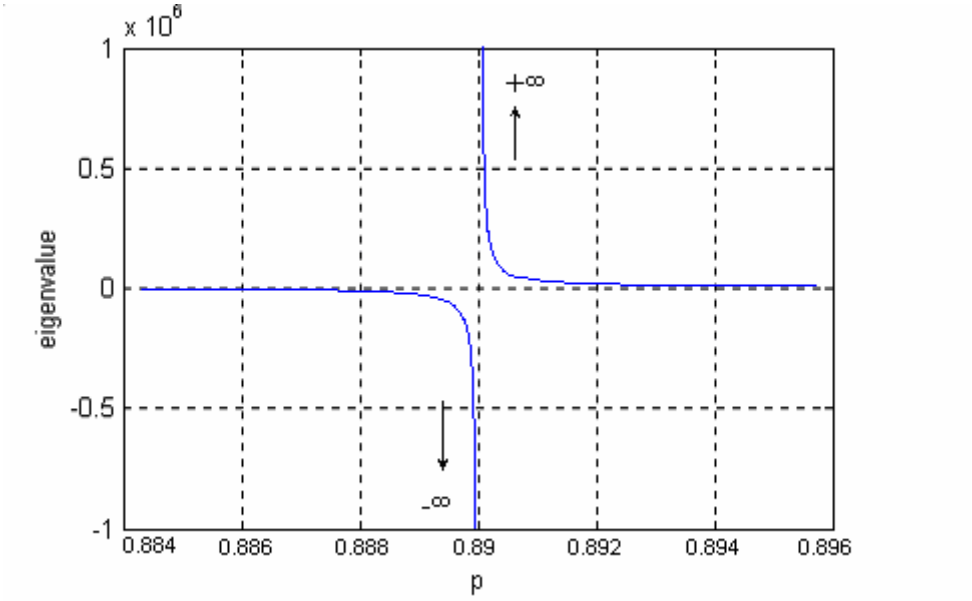

Fig. 35. The eigenvalues approach to infinity at SIB point C.

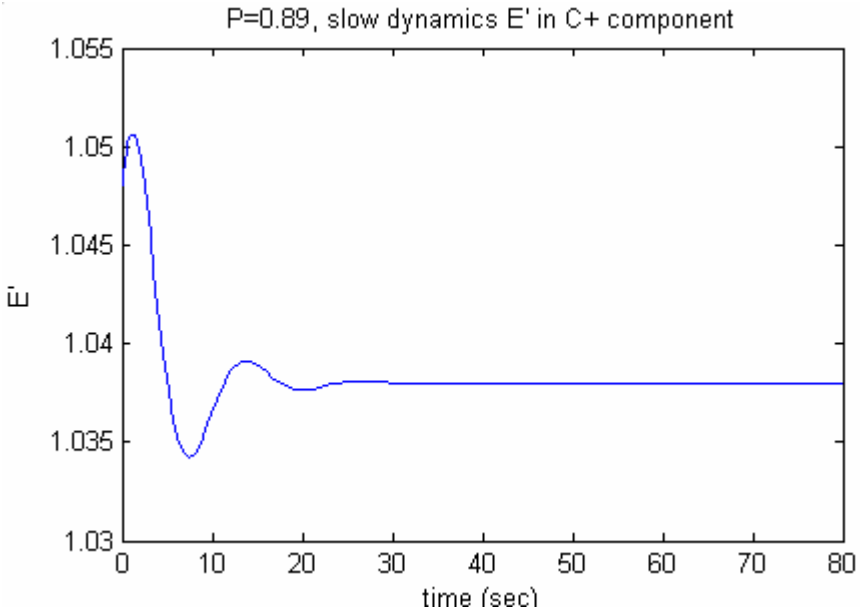

Fig. 36. Time response of *E'* initial at *E'*(0)=1.048.

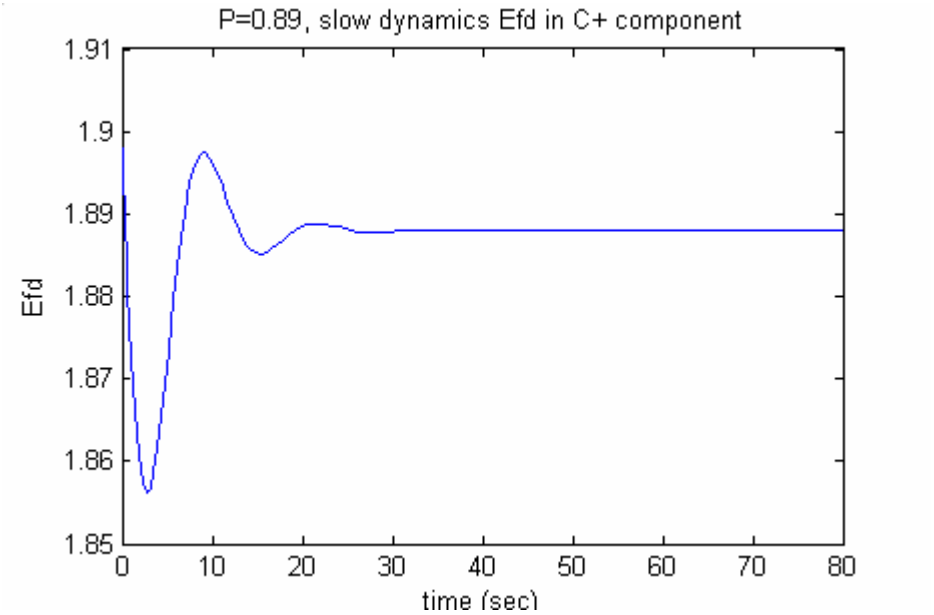

Fig. 37. Time response of E_{fd} initial at $E_{fd}(0)=1.9$.

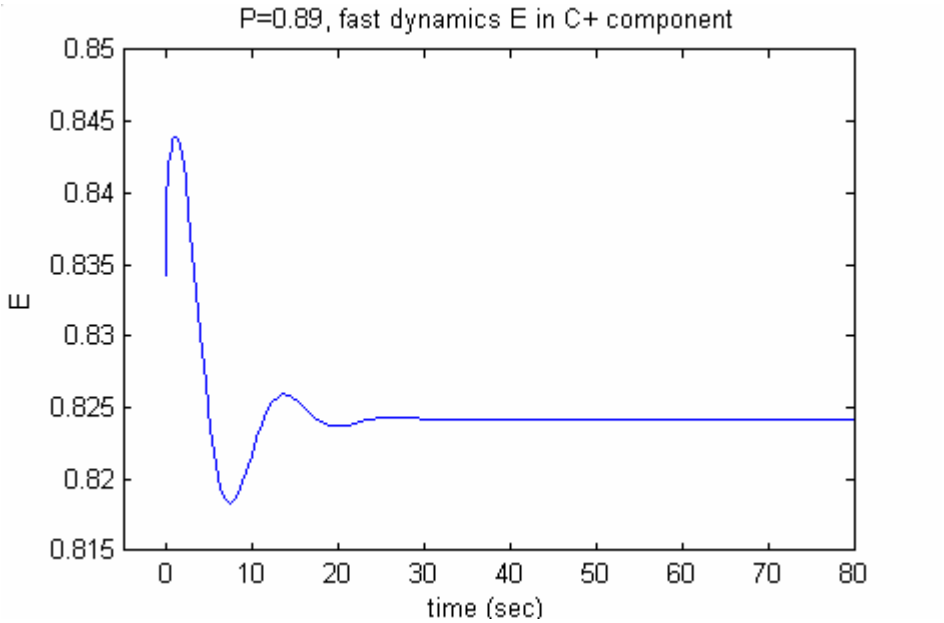

Fig. 38. Time response of E initial at $E(0)=0.834$.

As addressed in [19], the three bifurcations above play important roles in the dynamic analysis of power systems. The singularity-induced bifurcation C divides the system dynamics into two components C_+ and C_. In C_, the lower equilibrium is stable throughout C_ component but is typically not viable, mostly because of too low bus voltage for operation. A system break up by selective protection will follow. On the other hand, we should let the power system to operate in a practical region in the C+ component. The segment A-B-C (see Fig. 29) lies on the stability boundaries of the stable equilibrium points in C_+ component. These equilibrium points along the upper *P-V* curve are potential operating points of the power system. It should be observed that the region of attraction of such a stable equilibrium point, the usual operating point, gradually shrinks in size with increasing load and disappears when the Hopf bifurcation A is crossed. Changing system parameters of the excitation system and the transmission part may relocate the bifurcation points, thus improves the system dynamic properties.

The singularly perturbed ODE makes it easier to observe time responses and trace bifurcations. However, a singularly perturbed ODE might not preserve the bifurcation properties of the original DAE system. From the unreduced Jacobian J_u in (3.22), we see that the interactions between slow modes and fast modes are mainly driven by f_y and $g_y^{-1}g_x$. In fact, g_y^{-1} plays an important role in SIB. In [12], the fast dynamics is approximated by $-\frac{1}{\varepsilon}g_y{}^T g$ (we denote the method as TJM: Transpose Jacobian Method). When we use it in the power system example, the singular point C is no longer a singularity-induced bifurcation point. Fig. 39 shows that a break-away point

D is introduced on the left real axis of the eigenvalue plane. Observing in detail in TABLE VIII, we see that the fast modes are no longer fast when approaching point C. Looking into Fig. 39, we see that two eigenvalues moving along the negative real axis break away at point D and then move in the left half of the conjugate complex plane. They come back to real axis and meet at Point C. Point C becomes a break-in point with a zero eigenvalue. As *P* increases, one eigenvalue goes through zero and changes sign at point C. The stability property is changed at point C. However, system equilibrium points still exist beyond C. Point C is referred as a *saddle focus* bifurcation in the sense that a complex conjugate pair of eigenvalues merger into two real eigenvalues with opposite sign. So TJM does not preserve the bifurcation properties of the original DAE system. All these complicate the interaction picture between slow state variables and instantaneous variables and the identification of the voltage collapse point.

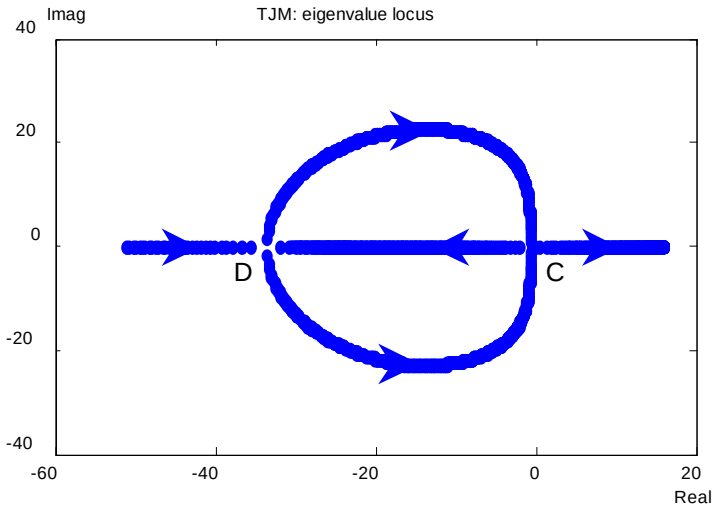

Fig. 39. Break-away point D and break-in point C.

TABLE VIII
A BREAK-AWAY POINT D INTRODUCED BY TJM AND POINT C BECOMES A BREAK-IN POINT

D	Eigenvalues	
	P=0.8795	P=0.8796
RJM	-20.2821 -0.3634	-20.9593 -0.3586
PTE	-99984.3184 -20. 1848 -0.3634	-99976.6428 -20.9651 -0.3586
TJM	-102.1177 -23.9438 -0.3614	-33.6534+j1.2319 -33.6534–j1.2319 -0.3585
C	Eigenvalues	
	P=0.8898	P=0.8899
RJM (SIB)	–1484. 0548 –0. 3482	1457.7860 –0. 3481
UJM (SIB)	–1506.7344 –0. 3482 –100000.7838	1437.1113 –0. 3480 –101438.6300
TJM	–0.8256+j0.9108 –0.8256–j0.9108 -0.2154	-2.0049 0.5141 -0.3759

3.3 Summary

By PTE technique, we convert a DAE to a singularly perturbed ODE. In addition, a simplified unreduced Jacobian matrix is also proposed. PTE makes all system variables involved explicitly to be observed. The time domain simulation is therefore easier to perform and the bifurcation properties are preserved. The traditional

substitution and reduction process to solve for a DAE system can be avoided using the proposed ODE form.

In power system dynamics, a very small ε is introduced to slow down the dynamic process of the power flow to observe the dynamic behaviors. An application of a dynamic voltage stability case is demonstrated to show that the proposed technique of PTE works well for both time domain simulation and bifurcation analysis.

CHAPTER IV

CONCLUSIONS

This thesis addresses some dynamic modeling issues of power system applications. We focus on the systematic descriptions and their applications, such as dynamic voltage stability issues in power systems etc. Mathematically, these kinds of problems are commonly modeled by differential-algebraic equations (DAE). In power system applications, the differential equations describe the slow dynamics, such as excitation control system, voltage regulators. The algebraic equations are corresponding to the power flow equations, which are fast modes compared with the slow modes of generation parts.

The objective of the thesis is to remodel the dynamic power system by an explicit state space form of ODE. Thus, we can quickly view the dynamic behaviors of the system by directly integrate the ODE since we do not need to solve the nonlinear algebraic equations.

To achieve our goal, we propose PTE technique to build the fast dynamics of the fast modes. Hence a DAE is converted to a singularly perturbed ODE. All system variables of slow modes and fast modes are involved in this ODE to be observed with their dynamic form.

Now, let us summarize our conclusions:

- The requirement of building the fast dynamics is that the fast dynamics converges fast to the algebraic constraints. The singularly perturbed ODE has the following explicit state space form:

$$\begin{cases} \dot{x} = f(x, y, p, \varepsilon) \\ \varepsilon\dot{y} = g^{FD}(x, y, p, \varepsilon) \end{cases}$$

where a very small ε is introduced to slow down the dynamic process of the power flow in order to observe the dynamic behaviors. We can directly integrate the ODE to observe the trajectories of dynamic responses without the reduction process.

- We present the technique of PTE (Perturb and Taylor's Expansion) to derive a general expression of fast dynamics. That is

$$\dot{y} = \frac{1}{\varepsilon} g^{FD} = -\frac{1}{\varepsilon} g_y^{-1} g$$

Using PTE, a DAE with *n* differential equations and *m* algebraic constraints is converted to a $(n+m)\times(n+m)$ dimensional ODE with the following form:

$$\begin{cases} \dot{x} = f(x, y, p, \varepsilon) \\ \dot{y} = -\frac{1}{\varepsilon} g_y^{-1} g \end{cases}$$

In addition, a simplified unreduced Jacobian matrix is proposed as below:

$$J_u = \begin{bmatrix} f_x & f_y \\ -\frac{1}{\varepsilon} g_y^{-1} g_x & -\frac{1}{\varepsilon} I_{m\times m} \end{bmatrix}$$

which is evaluated at each equilibrium point for tracing eigenvalues in the bifurcation analysis. We also introduce a simple way to avoid the calculation of

the inverse of the fast mode Jacobian. PTE preserves bifurcation properties of the original DAE system. An application of dynamic voltage stability is introduced to demonstrate that the approach works well without complicating the applications.

REFERENCES

[1] P. W. Sauer and M. A. Pai, *Power System Dynamics and Stability.* Upper Saddle River, NJ: Prentice-Hall, 1998.

[2] T. V. Cutsem, "Voltage instability: Phenomena, countermeasures, and analysis methods," *Proceedings of the IEEE*, vol. 88, Issue 2, pp. 208-227, Feb. 2000.

[3] C. W. Taylor, *Power System Voltage Stability.* New York: McGraw-Hill, Inc. 1994.

[4] C. Vournas, *Voltage Stability of Electric Power Systems.* Boston: Kluwer Academic Publishers, 1998.

[5] J. A. Momoh and M. E. El-Hawary, *Electric Systems, Dynamics, and Stability with Artificial Intelligence Applications.* New York: M. Dekker, 2000.

[6] P. M. Anderson, A. A. Fouad, *Power System Control and Stability.* Piscataway, NJ: IEEE Press, 1993.

[7] P. Kundur, *Power System Stability and Control.* New York: McGraw-Hill, 1994.

[8] G. M. Huang, L. Zhao, and X. Song, "A new bifurcation analysis for power system dynamic voltage stability studies," *Power Engineering Society Winter Meeting, 2002. IEEE*, vol. 2, pp. 882-887, Jan. 2002.

[9] G. M. Huang and K. Men, "Contribution allocation for voltage stability in deregulated power systems," *Power Engineering Society Summer Meeting, 2002 IEEE*, vol. 3, pp. 1290-1295, July 2002.

[10] H. Saadat, *Power System Analysis.* Boston: McGraw-Hill, 1999.

[11] Y. V. Makarof, I. A. Hiskens, and D. J. Hill, "Study of multisolution quadratic load flow problems and applied newton-raphson like methods," *IEEE International Symposium on Circuits and Syst.*, vol. 2, pp. 1508-1511, May 1995.

[12] B. W. Gordon and S. Liu, "A singular perturbation approach for modeling differential-algebraic systems," *ASME Journal of Dynamic Systems, Measurement, and Control*, vol. 120, pp. 541-544, Dec. 1998.

[13] P. Kokotovic, H. K. Khalil, and J. O'Reilly. *Singular Perturbation Methods in Control: Analysis and Design.* London: Orlando Academic Press, 1986.

[14] F. Colonius, L. Grüne, *Dynamics, Bifurcations, and Control.* New York: Springer-Verlag, Inc. 2002.

[15] S. Sastry, *Nonlinear Systems: Analysis, Stability, and Control.* New York: Springer-Verlag, Inc. 1999.

[16] R. A. Schlueter, S. Liu, and K. Ben-Kilani, "Justification of the voltage stability security assessment and diagnostic procedure using a bifurcation subsystem method," *IEEE Trans. Power Syst.*, vol. 15, pp. 1105-1111, Aug. 2000.

[17] V. Venkatasubramanian, H. Schaettler and J. Zaborazky, "Local bifurcations feasibility regions in differential-algebraic systems," *IEEE Trans. Automat. Cont.,* vol. 40, pp.1992-2013, Dec. 1995.

[18] V. Venkatasubramanian, H. Schaettler and J. Zaborazky, "Global voltage dynamics: study of a generator with voltage control, transmission and matched MW load," *The 29th IEEE CDC*, Honolulu, Hawaii, pp. 3045-3056, Dec.1990.

[19] V. Venkatasubramanian, H. Schattler, and J. Zaborszky, "Voltage dynamics: study of a generator with voltage control, transmission, and matched mw load," *IEEE Trans. Automat. Contr.*, vol. 37, pp.1717-1733, Nov. 1992.

[20] I. A. Hiskens and D. J. Hill, "Energy function, transient stability and voltage behavior in power systems with nonlinear loads," *IEEE Trans. Power Syst.,* vol. 4, pp. 1525-1533, Oct. 1989.

[21] J. H Chow, P. V. Kokotovic, and Robert J. Thomas, *System and Control Theory for Power Systems.* New York: Spring-Verlag, 1995.

[22] V. Venkatasubramanian, "Singularity induced bifurcation and the Van Den Pol oscillator," *IEEE Trans. Circuits Syst. I*, vol. 41, pp.765-769, Nov. 1994.

[23] IEEE Committee Report, "Excitation system model for power system stability studies," *IEEE Trans. Power Apparatus Syst*., vol. PAS-100, pp. 494-509, Feb.1981.

[24] L. H. Fink, *Bulk Power System Voltage Phenomena III Voltage Stability, Security, and Control.* Davos, Switzerland: ECC, Inc. August 1994.

VITA

Xuefeng Song was born in Dalian, China. His permanent address is: 87 Yongping Street, 18-4, Dalian, Liaoning 116021, P. R. China. He received his B.S. degree in mathematics at Shandong University and M.E. degree in electrical engineering at Dalian Maritime University, China, respectively in 1984 and 1996. He worked in Dalian Maritime University from 1987. He received his M.S. degree in electrical engineering at Texas A&M University in December 2003.